

POLITECNICO DI TORINO

Master's degree in Energy and Nuclear Engineering



A study of polarization induced Lanthanum Strontium Cobalt Ferrite (LSCF) - Erbium Stabilized Bismuth (ESB) cathode / Gadolinium Doped Ceria (GDC) electrolyte interface of reversible solid oxide cells

Supervisor:
Prof. Santarelli Massimo

Student:
Mr. Dealbera Emanuele

Academic Year 2019-2020

Index

1. Summary.....	5
2. Introduction	6
2.1 Prospect of electrochemical cell technologies.....	7
2.2 Reversible Solid Oxide Cells used as energy storage technologies.....	9
2.3 Operating principle.....	15
3. Literature review	18
3.1 Note of chemical thermodynamics.....	18
3.2 Galvanic cell.....	22
3.3 Electrolytic cell.....	25
3.4 Thermodynamics of electrochemical cells	27
3.5 Thermal flux management	46
3.6 High temperature solid oxide fuel cells (SOFC)	54
3.7 SOFC layers used in this study.....	60
4. Methods.....	63
4.1 Synthesis of LSCF decorated with ESB	63
4.2 Sintering of GDC electrolyte pellet	64
4.3 Fabrication of direct assembled LSCF-ESB on GDC.....	66
4.4 Electrochemical performance.....	67

5. Results and discussion	70
5.1 Impedance behaviour of LSCF cathode/GDC electrolyte	70
5.2 Impedance behaviour of LSCF-ESB cathode/GDC electrolyte	75
5.3 Microstructure of electrode/electrolyte interface	80
6. Conclusion.....	87
7. Acknowledgements	89
8. Appendix.....	90
9. References.....	92

1. Summary

Lanthanum Strontium Cobaltite Ferrite (LSCF) decorated with Erbium-Stabilized Bismuth (ESB) ($\text{La}_{0.6}\text{Sr}_{0.4}\text{Co}_{0.2}\text{Fe}_{0.8}\text{O}_{3-\delta}\text{-Er}_{0.4}\text{Bi}_{1.6}\text{O}_3$) directly applied on Gadolinium-Doped Ceria (GDC) electrolyte ($\text{Gd}_{0.1}\text{Ce}_{0.9}\text{O}_{1.95}$) cell was fabricated, tested and analysed after 100 h of polarization with cathodic current of 1000 mAcm^{-2} at 750°C . Results show a larger segregation and migration of Erbium with a similar even if smaller behaviour for Bismuth after polarisation. This mechanism leads to a reduction of impedance across the sample and consequently to lower losses in term of power for reversible Solid Oxide Cell (rSOC) application. Results are compared with pristine LSCF to highlight the higher performance with the decoration.

2. Introduction

Reversible Solid oxide cells (rSOCs) are electrochemical energy conversion devices to convert chemical energy of fuels such as hydrogen, natural gas to electricity with high efficiency and low greenhouse emission as compared to conventional power generation plants. RSOCs generally operate at high temperatures of 900-1000°C which lead to high system costs and performance degradation [1]. Therefore, decreasing the operating temperature will provide more opportunities for the material selection and decreasing fuel cells' cost to allow them competitive with traditional power generation system. However, reducing the operation temperature would result in an increase of ohmic resistance of electrode and electrolyte and electrode polarization losses at the electrode/electrolyte interface in the cell. One possible solution could be the utilization of new materials with higher electrical and ionic conductivity at lower temperature. This is the case of large percentage of total polarization losses related to the cathode electrode-electrolyte interface. The focus of this work is to investigate the polarization induced interface at the lanthanum strontium cobalt ferrite ($\text{La}_{0.6}\text{Sr}_{0.4}\text{Co}_{0.2}\text{Fe}_{0.8}\text{O}_{3-d}$, LSCF) decorated with erbium-stabilized bismuth oxide ($\text{Er}_{0.4}\text{Bi}_{1.6}\text{O}_3$, ESB) cathode and gadolinium-doped ceria ($\text{Gd}_{0.1}\text{Ce}_{0.9}\text{O}_{1.95}$, GDC) electrolyte of solid oxide fuel cells and the electrochemical performance under solid oxide fuel cells operation conditions.

2.1 Prospect of electrochemical cell technologies

An electrochemical cell system is able to convert chemical energy into electrical energy and vice versa. This system can be used in fuel cell (FC) mode to produce electrical energy starting from a stream of mass characterized by high value of Gibbs free energy or in electrolysis cell (EC) mode to produce chemicals using electricity. The classical way to take advantage of chemical energy in order to generate electrical power is to produce heat at high temperature through combustion, convert it into mechanical energy using a thermodynamic cycle and produce electrical power through an alternator. This is a very inefficient and more complex way to exploit chemical energy than electrochemical cells as they are able to directly convert chemical energy into electrical one, ensuring low value of Σ_{irr} and high efficiency.

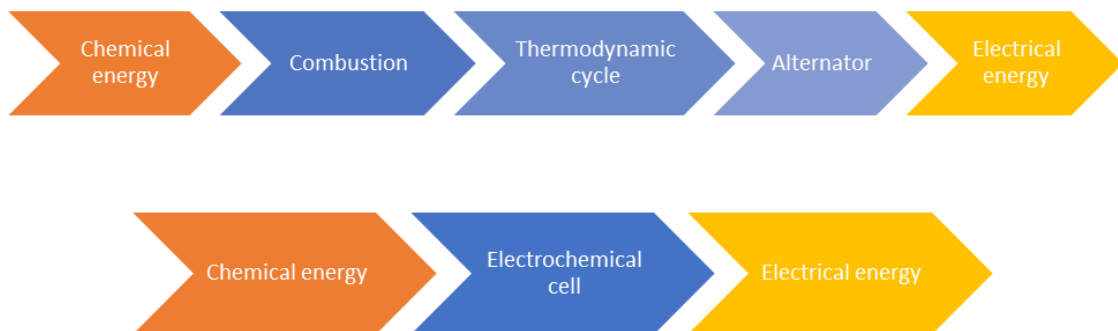


Figure 1 Schematic transformation of energy using an ICE (top) or a FS (bottom)

Fuel cells can be categorized depending on the material composing the electrolyte, which limits the temperature range of operations. As shown in Figure 1, starting from the high temperature solid oxide fuel cells (SOFCs) operate at 800-1000°C; at temperatures between 600-650°C molten carbonate fuel cells (MCFCs) are suitable;

decreasing the temperature, phosphoric acid fuel cells (PAFCs), proton exchange membrane fuel cells (PMFCs) and alkaline fuel cells (AFCs) are used. Increasing operation temperature will increase the efficiency, but the drawbacks are higher system complexity, the material cost and higher cell fabrication cost [2]. Herein only Solid Oxide Fuel Cells (SOFCs) are taken into account.

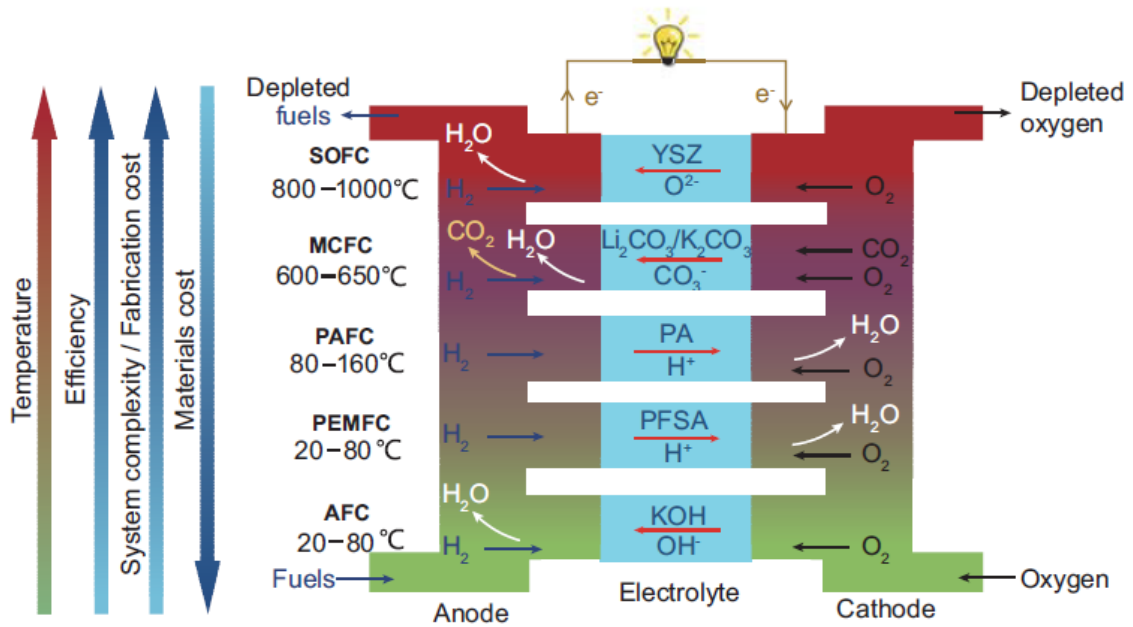


Figure 2 Fuel cell types, showing the general trend in the relationship between the operation temperature, efficiency, system complexity, fabrication cost and materials cost of the FC technologies [2].

Another positive side of rSOCs could be found in the energy storage: the enhancement of power generated through renewable energy, like solar and wind sources, provides opportunity to reduce fossil fuel utilization and mitigate greenhouse gas emission. To increase the availability of RES (renewable energy sources) it became necessary to deal with the intermittence of these sources: a way to store energy which makes possible to release it when required is mandatory. Due

to the fact that rSOCs can be used in both fuel cell mode and electrolysis mode, they are very attractive as possible solution to this problem.

2.2 Reversible Solid Oxide Cells used as energy storage technologies

In 2008, the European Union signed a first step for the fight against climate change. The package, known as 20 - 20 - 20 objectives, requires achieving 20 % of use energy coming from renewable energy sources, 20 % of reduction on primary energy consumption and 20 % of greenhouses gasses less than 1990's levels by 2020. The European commission has then required to achieve the target of 40 % reduction of greenhouse gasses compared to 1990's levels, an increment of 27 % of energy consumption coming from the renewable sector and 27 % of energy savings [3]. To complete these tasks, main measures to be implemented are the energy efficiency improvement, both in building constructions and in power generation sector; a deep exploitation of renewable energy sources (RES); carbon capture and sequestration / utilization from industrial emitters and fossil power plants.

In this work, the focus will be kept on the renewable energy sources and the main problem related to this kind of technologies is the intermittence of the resources. The generation from renewable energy takes into account different kind of energy such as solar energy, wind energy, geothermal energy and hydroelectric energy. Due to its heterogeneity, it can be noticed that the energy generated from renewable

sources is not constant along the day: there is a peak when the Sun is high in the sky and the energy from solar power plants is larger. The principal issue related to the energy production exploiting an energy source such as the Sun, is the intermittent nature of these sources. There is a gap between production and request: there is a discrepancy between the energy coming from RES - based systems and the requested power from the load. Figure 3 shows the energy generation coming from wind power plants located in the south of Italy during the month of January 2019 in comparison with the electrical national load. All the data are available on Terna website [4].

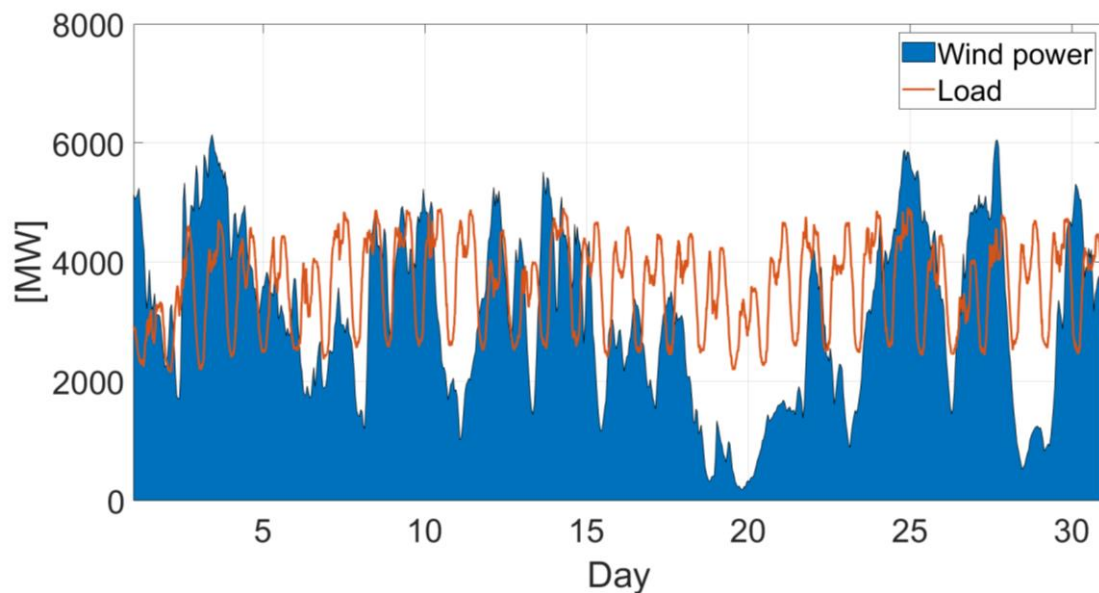


Figure 3 Wind power and electrical load in Italy during January 2019; data come from Terna [4]

There are periods when the wind power is higher compared to the required load and other moments with the opposite situation. Wind power plants are only one example: this can be generalized to all the renewable energy sources and translated

in periods of overproduction of energy from RES systems and period of energy shortage of the users. In order to dampen and control these negative effects, a grid management improvement in terms of transmission capacity and storage capacity is required. Increasing the grid connection will result in an easier and much more immediate energy transport. This means that if the energy demand cannot be satisfied by local production, energy can be easily supplied from the grid. Increasing grid connection reduces both daily and seasonal fluctuation of the generation and load curve: the disequilibrium between produced and required energy is reduced thanks to a faster reply of the grid.

The storage capacity will affect the disequilibrium between produced and required energy in a similar way as transport capacity does: it will reduce the excess, moving the difference between production and request towards the equilibrium point. A large storage system allows to not waste the energy surplus in case of overproduction.

At this point, reversible solid oxide cell technologies acquire a certain interest due to the high capability to transform electrical energy into chemical energy, that can be stored as gas (e.g. H₂), and, vice versa, to produce electrical energy starting from chemical energy.

A possible pathway from renewable energy sources to the electric grid passing through the chemical storage could be using of electrolytic cells for electrolysis: hydrogen can be produced and stored. Then, starting from the stored gas, the electricity intake can be performed. This system, known as power to power (P2P), is shown in figure 4: the advantages of this solution can be found in a reduction of fossil consumption that takes to a lower pollutants emission; P2P allows to reduce

cost of energy production through fossil fuels, considering only the energy transportation and management as cost; the energy security and the grid reliability are improved.

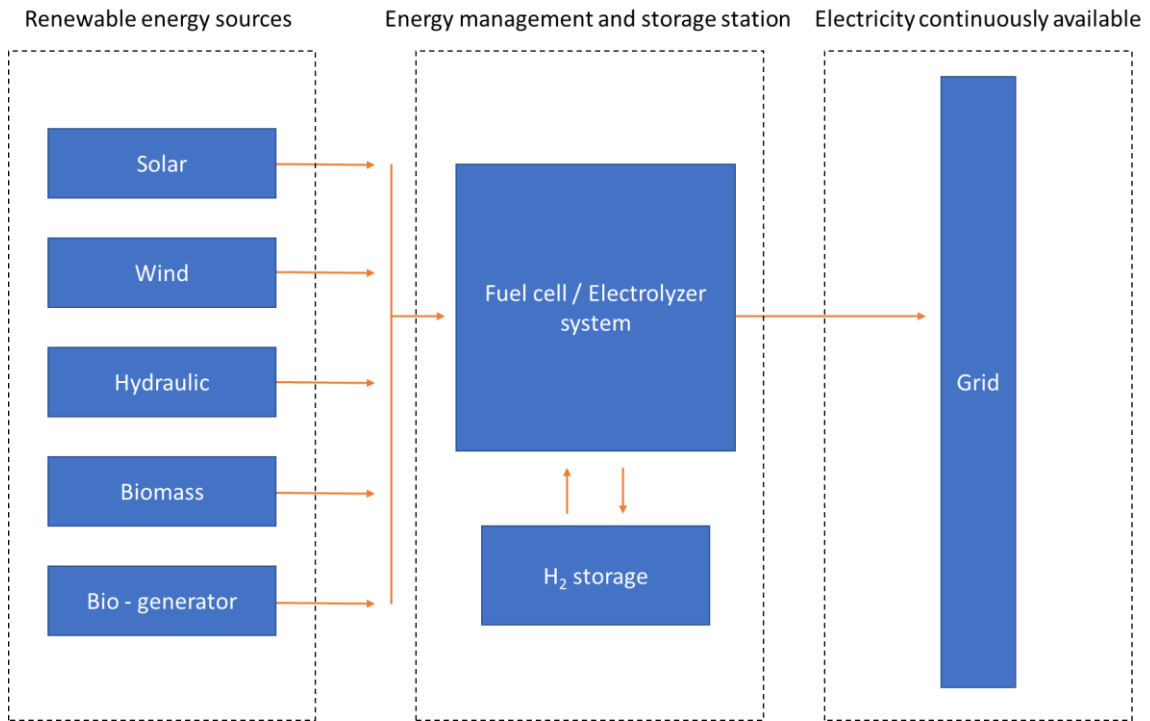


Figure 4 Power to Power (P2P)

Numerical analysis and a more general concept behind P2P and P2G technologies were well explained by Domenico Ferrero et al. [5]. In the paper, a techno-economic assessment of Power to Gas (P2G) was done, investigating the possibility for variable Renewable Energy storage into hydrogen through low and high temperature (PEM and SOEC) water electrolysis technologies. The study was performed for three different applications of the RES-produced hydrogen: injection in the natural gas grid, production of electricity with a P2P system and on-site

vehicle fuelling for mobility. Results show that in a 2030 scenario the levelized cost of electricity produced with these technologies is sensibly lower respect to other kind of storage system as Compressed Energy Storage (CAES) or batteries. The cost of hydrogen for mobility and grid injection will be very similar for all the technological options, with a very strong cost reduction (90%) for the SOEC-based option. System based on SOEC and alkaline fuel cells will achieve a round-trip efficiency of 46%.

International projects concerning fuel cells and hydrogen technologies are regulated by the European Government through Horizon 2020, which is the Framework Programme according to which all FCH JU projects financed under the 2014-2020 call for proposals are funded [6]. Here, the main projects related to energy and transport are collected and explained: in this work, only the projects mostly related to hydrogen production and storage are quoted.

REMOTE, “Remote area Energy supply with Multiple Options for integrated hydrogen-based Technologies” [7] is aimed to demonstrate the technical and economic feasibility of two fuel cells-based H₂ energy storage solutions: one integrated P2P system and one non-integrated P2G+G2P system (Power to Gas and Gas to Power). The idea is to exploit renewable energy coming from sun, biomass, water and wind to produce hydrogen that can be used for mobility or stored for a following generation of electricity. The hydrogen synthesis can be obtained with reversible Solid Oxide Cells, that are also able to convert the gas into electricity. Figure 5 shows the principle behind REMOTE project.

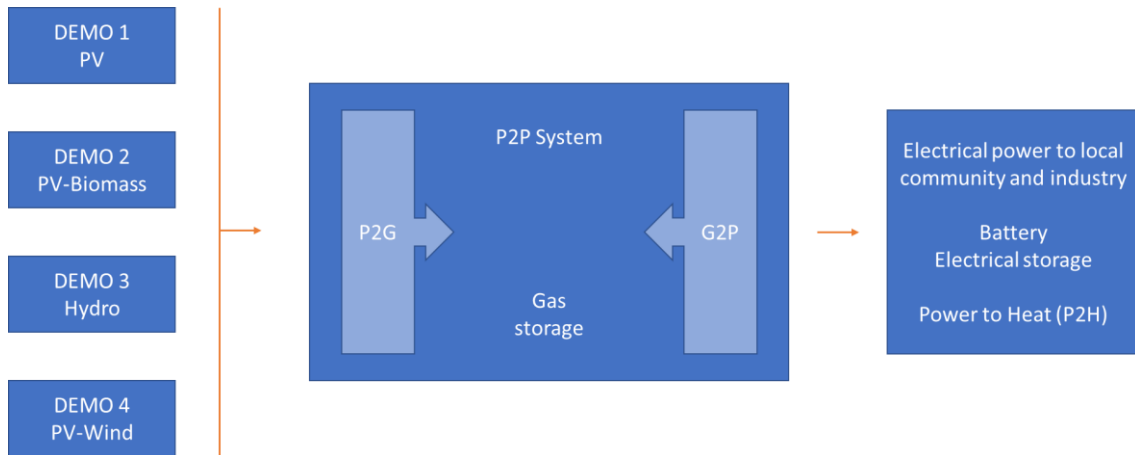


Figure 5 Schematic concept of REMOTE project

NEPTUNE, Next Generation PEM Electrolyser under New Extremes [8] starts from the concept that water electrolysis supplied by renewable energy is the foremost technology for producing “green” hydrogen for fuel cell vehicles. The ability to follow rapidly an intermittent load makes this an ideal solution for grid balancing. To achieve large-scale application of PEM electrolyzers, a significant reduction of capital costs is required together with a large increase of production rate and output pressure of hydrogen, while assuring high efficiency and safe operation. To address these challenges, a step-change in PEM electrolysis technology is necessary. The NEPTUNE project develops a set of breakthrough solutions at materials, stack and system levels to increase hydrogen pressure and current density for the base load, while keeping the nominal energy consumption.

REFLEX, Reversible solid oxide Electrolyzer and Fuel cell for optimized Local Energy miX [9], which aims at developing an innovative renewable energies storage solution, the “Smart Energy Hub”, based on reversible Solid Oxide Cell (rSOC) technology. The challenging issue of achieving concomitantly high efficiency, high

flexibility in operation and cost optimum is duly addressed through improvements of rSOC components (cells, stacks, power electronics, heat exchangers) and system, and the definition of advanced operation strategies.

Haeolus, Hydrogen-aeolic energy with optimised electrolysers upstream of substation. This project consists of the installation of a PEM electrolyser with a capacity of 2 MW in the remote region of Varanger, Norway, inside the Raggovidda wind farm, whose growth is limited by grid bottlenecks. The electrolyser is integrated with the wind farm, hydrogen storage and a smaller fuel cell for re-electrification.

2.3 Operating principle

A solid oxide fuel cell is a system that takes advantage of a chemical reaction. An example could be a battery in discharge. The same system can work in the opposite way, as the battery in recharge mode: the energy is converted from chemical energy to electrical energy and vice versa.

The aim of a SOFC is to make happen the reactions (oxidation and reduction) taking places into the electrode, letting the ions pass through the electrolyte and making the electrons pass through an external circuit.

The electrochemical cell is composed by two electrodes: the anode, where the oxidation reaction occurs (delivery of free electrons); and the cathode, where the reduction reaction occurs (gain of free electrons) and electrolyte layer, which physically separates anode and cathode and should be characterised by very low

molecular diffusivity and capability to conduct electrons and a very high capability to conduct ions.

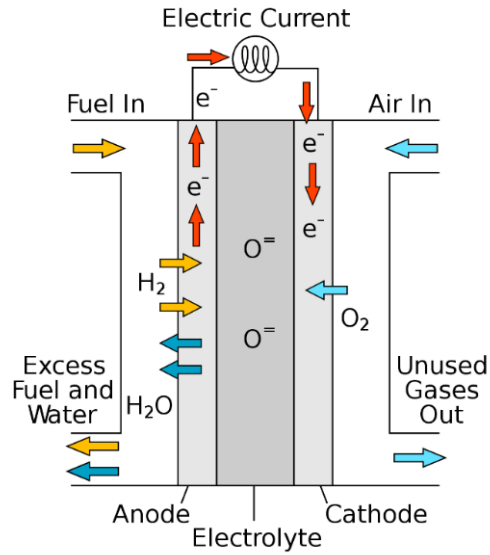
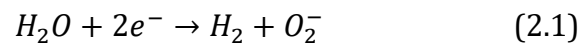


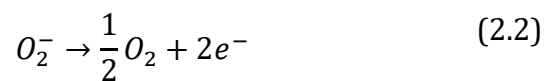
Figure 6 Scheme of a Solid Oxide Fuel Cell [10]

The electrochemical cell can be analysed using the two reactions that happen in the cathodes.

The reaction of reduction occurring at the anode is:



While at the cathode, the reaction of oxidation is:



Combining together these two equations, the whole reaction is obtained:



The global reaction occurs because the ions can travel through the electrolyte layer and the electrons can travel in an external circuit. A charge separation occurs between the two electrodes generating a voltage differential ΔV . Closing the external circuit, the equilibrium is broken and a current I is generated due to the electrons flow. The presence of a current flowing through a voltage gradient generates an electrical power.

3. Literature review

In this section a remind of the basic principle according to a reversible Solid Oxide Cell works and an overview of electrochemical losses were done.

The equations that regulate the reactions were written taking contents from “High Temperature Solid Oxide Fuel Cells – Fundamentals, Design and Applications” [11] and using knowledges acquired during classes at Politecnico di Torino.

3.1 Note of chemical thermodynamics

An electrochemical cell is a device that transform chemical energy to electrical energy starting from a fuel (e.g. H_2) and an oxidant (air). This system can be considered in terms of free enthalpy of the reaction of fuel with the oxidant. The other term that must be taken into account is the heat: a SOFC system produces heat that has to be removed to avoid problems culminating in the breakdown of the cell.

A reversible fuel cell can be described using the first and second laws of thermodynamic. Let's consider an infinitesimal modification of the degree of advancement of the reaction $d\xi$ nearly the equilibrium state.

First law of thermodynamics:

$$\delta Q - \delta L = \frac{dU}{d\xi} \quad (3.1)$$

where δQ is the infinitesimal amount of heat,

δL is the infinitesimal amount of work,

dU is the variation of internal energy,

$d\xi$ is the variation of degree of reaction.

Second law of thermodynamics:

$$\delta Q \leq T \cdot \frac{ds}{d\xi} \quad (3.2)$$

where ds is the variation of entropy.

The expression of δQ is derived from the first law and, substituting it in the second law, the following expression is obtained:

$$\delta Q = \delta L + \frac{dU}{d\xi} \leq T \cdot \frac{ds}{d\xi} \quad (3.3)$$

$$\delta L \leq T \cdot \frac{ds}{d\xi} - \frac{dU}{d\xi} \quad (3.4)$$

By definition, the infinitesimal work can be written as:

$$\delta L = p \cdot \frac{dV}{d\xi} \quad (3.5)$$

where p is the pressure at which the reaction occurs and dV is the infinitesimal variation of volume.

Also, by definition, the Gibbs free energy G can be written as following:

$$H = U + p \cdot V \quad (3.6)$$

$$G = H - T \cdot s \quad (3.7)$$

$$G = U + p \cdot V - T \cdot s \quad (3.8)$$

where H is the enthalpy,

U is the internal energy,

p is the pressure,

V is the volume,

T is the temperature,

s is the entropy.

The infinitesimal variation of Gibbs free energy can be obtained and substituted in the expression of infinitesimal work deduced before:

$$\frac{dG}{d\xi} = \frac{dU}{d\xi} + p \cdot \frac{dV}{d\xi} + V \cdot \frac{dp}{d\xi} - T \cdot \frac{ds}{d\xi} - s \cdot \frac{dT}{d\xi} \quad (3.9)$$

$$T \cdot \frac{ds}{d\xi} = \frac{dU}{d\xi} + p \cdot \frac{dV}{d\xi} + V \cdot \frac{dp}{d\xi} - s \cdot \frac{dT}{d\xi} - \frac{dG}{d\xi} \quad (3.10)$$

$$p \cdot \frac{dV}{d\xi} \leq \frac{dU}{d\xi} + p \cdot \frac{dV}{d\xi} + V \cdot \frac{dp}{d\xi} - s \cdot \frac{dT}{d\xi} - \frac{dG}{d\xi} - \frac{dU}{d\xi} \quad (3.11)$$

Simplifying, the following expression is obtained:

$$0 \leq V \cdot \frac{dp}{d\xi} - s \cdot \frac{dT}{d\xi} - \frac{dG}{d\xi} \quad (3.12)$$

The reaction takes place at a fixed pressure and temperature, so the infinitesimal variation of these terms is equals to zero.

The obtained expression:

$$\frac{dG}{d\xi} \leq 0 \quad (3.13)$$

means that, nearby the equilibrium state, the Gibbs free energy is always decreasing.

At the equilibrium state, the Gibbs free energy is equal to zero.

$$\frac{dG}{d\xi}_{equilibrium} = 0 \quad (3.14)$$

The sign of the variation of Gibbs free energy ΔG gives information about the spontaneity of a reaction: a negative amount of ΔG means that the reaction will occur spontaneously (e.g. a battery in discharge mode: the system will provide electrical energy using chemicals without any need of an external help); while a positive quantity of ΔG will characterize a reaction that needs to absorb energy in order to happen (e.g. a battery in recharge mode: the system will recharge itself only with an external electrical source).

Using the variation of Gibbs free energy ΔG to differentiate two different situations, it becomes possible consider an electrochemical cell as galvanic cell or electrolytic cell.

3.2 Galvanic cell

A galvanic cell is a system in which the disequilibrium of reactants in terms of Gibbs free energy is directly transformed into electrical power. This system is characterized by a ΔG lower than zero: this means that there will be a spontaneous reaction inside of the cell and electrical power will be able to be generated starting from chemicals.

A system operating in steady state conditions is considered: figure 7 shows the most generic case.

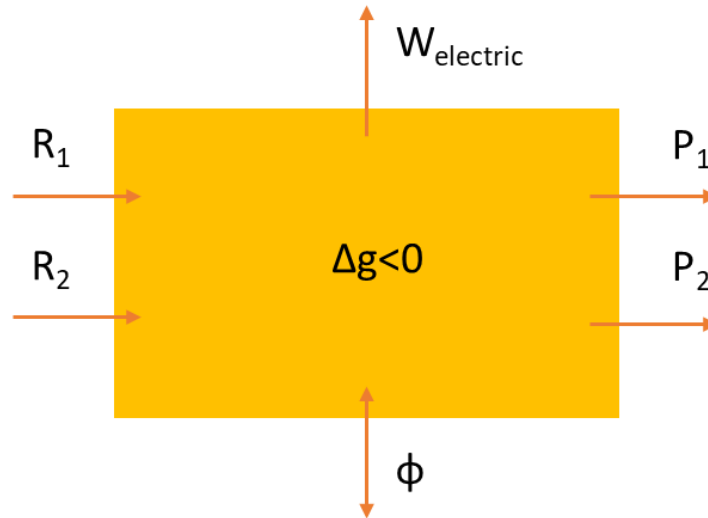


Figure 7 Control volume for a galvanic cell

First and second law of thermodynamics are applied to the control volume.

First law $\left[\frac{J}{mol}\right]$:

$$\bar{q} - \bar{l}_{el} = \sum_{product} \nu_p \bar{h}_p(T, p_i) - \sum_{reactant} \nu_r \bar{h}_r(T, p_i) \quad (3.15)$$

where \bar{q} is the heat flux Φ normalized by the chemical species oxidized at the anode

\dot{n}_{fuel} ;

\bar{l}_{el} is the electrical work W_{el} normalized by the chemical species oxidized at the anode \dot{n}_{fuel} ;

ν is the stoichiometric coefficient obtained from the chemical species normalized by

the chemical species oxidized at the anode $\left(\frac{\dot{n}_p}{\dot{n}_{fuel}}, \frac{\dot{n}_r}{\dot{n}_{fuel}}\right)$;

\bar{h} is the enthalpy evaluated at given temperature and partial pressure.

Second law $\left[\frac{J}{mol}\right]$:

$$\frac{\bar{q}}{T} - \xi_{irr} = \sum_{product} \nu_p \bar{s}_p(T, p_i) - \sum_{reactant} \nu_r \bar{s}_r(T, p_i) \quad (3.16)$$

where ξ_{irr} is the irreversible entropy end in this specific case it is equal to zero due to the absence of transport phenomena;

\bar{s} is the entropy.

Combining together the first and second laws of thermodynamics, an expression of the specific electrical work is gained:

$$\bar{l}_{el} = - \left\{ \left[\sum_{product} \nu_p \bar{h}_p(T, p_i) - \sum_{reactant} \nu_r \bar{h}_r(T, p_i) \right] - T \left[\sum_{product} \nu_p \bar{s}_p(T, p_i) - \sum_{reactant} \nu_r \bar{s}_r(T, p_i) \right] \right\} \quad (3.17)$$

That corresponds to:

$$\bar{l}_{el} = -[\Delta \bar{h}_{reaction} - T \Delta \bar{s}_{reaction}] \quad (3.18)$$

$$\bar{l}_{el} = -\Delta\bar{g}_{reaction} \quad (3.19)$$

The final expression says that the electrical work obtainable from an electrochemical cell is the opposite of the difference of Gibbs free energy corresponding to that specific reaction.

Considering the case of a galvanic cell, where $\Delta\bar{g}_{reaction} < 0$, the electrical work is positive: starting from chemicals, it is possible to obtain positive electrical work exploiting a spontaneous reaction.

3.3 Electrolytic cell

An electrolytic cell is a system that requires electrical power to make happen a non-spontaneous reaction (e.g. water electrolysis). Figure 8 shows the general black box approach to an electrolytic cell and, using the same procedure as before, it is possible to write the laws of thermodynamics for this system.

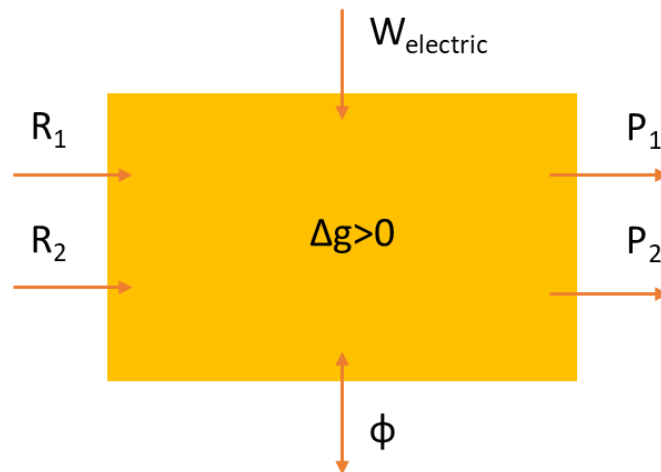


Figure 8 Control volume for an electrolytic cell

First law and second law combined together give the expression of the specific electrical work as for the galvanic cell:

$$\bar{l}_{el} = -[\Delta\bar{h}_{reaction} - T\Delta\bar{s}_{reaction}] \quad (3.20)$$

$$\bar{l}_{el} = -\Delta\bar{g}_{reaction} \quad (3.21)$$

In the case of electrolytic cell, the difference in terms of Gibbs free energy is positive: this means that the electrical work is negative and has to be provided to make the reaction happen.

3.4 Thermodynamics of electrochemical cells

A review of thermodynamics principles that give the rules for the electrolytic cells is made in this section. To describe the electrochemical performance of the cell, the values of current and voltage have to be analysed. There is a relation between the molar flow rate of species reacting at the electrodes and the current flowing in the external circuit. The Faraday's law is used to obtain this relation expressed in mol per second and it is shown in the (3.22):

$$\dot{n}_r = \frac{I}{z_r \cdot F} \quad (3.22)$$

Exploiting the molar weight of the reactant species, a relation involving the mass flow rate expressed in grams per second is obtained:

$$\dot{m}_r = \frac{I}{z_r \cdot F} \cdot PM_r \quad (3.23)$$

where \dot{m}_r is the mass flow rate;

I is the current;

z_r is the charge number of species "r": this is the number of electrons exchanged in an electrochemical reaction (oxidation or reduction) of the species "r" per molecule (number of electrons delivered/gained by oxidation/reduction of 1 mol of reactants);

F is the Faraday's constant equal to $96487 \left[\frac{C}{mol} \right]$;

PM_r is the molecular weight of species "r".

Faraday's law is obtained (for a galvanic cell) considering that the reaction of 1 mol of H_2 will produce 2 electrons:



Considering the number of Avogadro $N_a = 6,022 \cdot 10^{23} \left[\frac{1}{mol} \right]$, the reaction of 1 molecule of H_2 will produce $2N_a$. The charge associated to $2N_a$ electrons is:

$$C = 2 \cdot N_a \cdot q_e \quad (3.25)$$

where C is the charge;

q_e is the charge of one electron equal to $1,6 \cdot 10^{-19} [C]$;

The product between the number of Avogadro and the charge of one electron gives the value of Faraday's constant.

As the current is defined as the number of charges q moving in the unit time, a molar flow rate of reactants will generate a current:

$$I = 2F \cdot \dot{n}_{H_2} \quad (3.26)$$

using hydrogen as example.

Before starting to speak about the electrochemical potential ΔV , the conductivity of electrolytes has to be introduced. An electrolyte layer must have good quality as ions conductors while the electric conductivity should have a value as low as possible. Therefore, as far as electrolytes are concerned, the ionic conductivity is the most relevant parameter that is taken into account. It can be expressed for a generic ionic species i with:

$$\sigma_{ion,i} = z_i^2 \cdot F^2 \cdot C_i \cdot \mu_i \quad (3.27)$$

where $\sigma_{ion,i}$ is the ionic conductivity for the species i expressed in $\left[\frac{S}{m}\right]$ where S corresponds to Siemens $\left[\frac{1}{\Omega}\right]$;

z_i is the charge number of the ions;

F is the Faraday's constant;

C_i is the concentration of ions inside the material $\left[\frac{mol}{m^3}\right]$;

μ_i is the ionic mobility equal to the ratio between the speed and the electric field of

$$1 \text{ volt per meter } \frac{\left[\frac{m}{s}\right]}{\left[\frac{V}{m}\right]} = \left[\frac{m^2}{s} \cdot m\right].$$

As far the electrochemical has to follow the charge conservation, the current that flows in the external circuit has to be equal to the numbers of ions flowing in the electrolyte from electrode to electrode. But the electric conductivity of the external circuit has a very lower value respect the ions conductivity of the electrolyte:

$$\sigma_{ion} \ll \sigma_{e^-} \quad (3.28)$$

Considering together all the information, the ohmic drop across the cell is expressed with the simple law for the electric potential:

$$\Delta V = R \cdot I = \frac{1}{\sigma} \cdot I \quad (3.29)$$

Knowing that (3.28) the following comparison can be made:

$$\Delta V_{electrolyte} = \frac{I_{ion}}{\sigma_{ion}} \quad (3.30)$$

$$\Delta V_{external\ circuit} = \frac{I_{e^-}}{\sigma_{e^-}} \quad (3.31)$$

$$\Delta V_{electrolyte} \gg \Delta V_{external\ circuit} \quad (3.32)$$

The ohmic drop across the external circuit has a lower value compared to the one taking place in the electrolyte: this behaviour is due to high difficulty of ions to cross the electrolyte layer that means a low conductivity. To avoid this bad effect, the thickness of the electrolyte layer is reduced as much as possible.

In this section, the cell is considered as a black box: the focus is only concentrated on what enters and exits in/from the cell and not on what happens inside of the system. The other hypothesis are the conditions of equilibrium, that means that the cell will operate with reversibility, and steady state conditions. Considering a Gibbs

free energy variation ΔG lower than zero, the electrolytic cell will work as galvanic cell. The first and second law of thermodynamics (3.15) and (3.16) are normalised by the molar flow rate of fuel \dot{n}_{fuel} , obtaining the expression of the molar electric work in reversible conditions (3.17).

The same term can be extrapolated from the Faraday's law seen before in the (3.22):

$$\bar{l} = \frac{W_{el}}{\dot{n}_{fuel}} = \frac{I \cdot OCV}{\frac{I}{z_r \cdot F}} = z_r \cdot F \cdot OCV \quad (3.33)$$

An electrochemical cell can work in reversible conditions only if there is the situation of open circuit voltage (OCV). If the circuit is open, no transport phenomena will occur and there is no generation of entropy and combining equations (3.21) and (3.22) the Nernst equation in reversible conditions is obtained:

$$OCV = -\frac{\Delta g_{react}}{z_f \cdot F} \quad (3.34)$$

The larger Δg_{react} , the higher voltage drop that can be generated. Since the Δg_{react} is a function of temperature and pressure which the cell operates at, the open circuit voltage becomes function of the same parameter too.

Analysing the variation of OCV in relation with the temperature, if Δg_{react} is decreased with a decrement of the temperature, also the OCV will have lower value corresponding to lower value of temperature.

The other parameter that can modify the value of OCV is the pressure which the cell operates at. Assuming the ideal behaviour of the gases involved in the reaction, the Gibbs free energy for a generic species i can be expressed as follows:

$$\bar{g}_i(T, P_i) = \bar{g}_i(T, P_0) + \bar{R}T \ln \left(\frac{P_i}{P_0} \right) \quad (3.35)$$

Substituting (3.34) into (3.33), a new expression for OCV is obtained:

$$\begin{aligned} OCV_{galvanic\ cell} &= -\frac{\Delta g_{react}(T, P_i)}{z_f \cdot F} \quad (3.36) \\ &= -\frac{\Delta g_{react}(T, P_i)}{z_f \cdot F} \\ &\quad + \frac{\bar{R}T}{z_f \cdot F} \ln \left[\frac{\sum_i^{reactants} \left(\frac{P_i}{P_0} \right)^{\nu_i}}{\sum_i^{products} \left(\frac{P_i}{P_0} \right)^{\nu_i}} \right] \end{aligned}$$

In this form, the Nernst equation is composed by terms depending on the temperature separated from terms depending on pressure.

The value of open circuit voltage can be increased acting on the partial pressure in the following way: an enhancement of partial pressure of reactants by increasing the molar fraction and/or the total pressure; a decrease of partial pressure of product by decreasing the molar fraction and/or the total pressure.

All these evaluations can be done as well as for an electrolytic cell: the sign before Δg_{react} is plus instead of minus as for a galvanic cell, so the expression becomes

$$\begin{aligned}
OCV_{electrolytic\ cell} &= + \frac{\Delta g_{react}(T, P_i)}{z_f \cdot F} & (3.37) \\
&= + \frac{\Delta g_{react}(T, P_i)}{z_f \cdot F} \\
&\quad - \frac{\bar{R}T}{z_f \cdot F} \ln \left[\frac{\sum_i^{reactants} \left(\frac{P_i}{P_o}\right)^{v_i}}{\sum_i^{products} \left(\frac{P_i}{P_o}\right)^{v_i}} \right]
\end{aligned}$$

$$\begin{aligned}
OCV_{electrolytic\ cell} & & (3.38) \\
&= + \frac{\Delta g_{react}(T, P_i)}{z_f \cdot F} \\
&\quad + \frac{\bar{R}T}{z_f \cdot F} \ln \left[\frac{\sum_i^{products} \left(\frac{P_i}{P_o}\right)^{v_i}}{\sum_i^{reactants} \left(\frac{P_i}{P_o}\right)^{v_i}} \right]
\end{aligned}$$

The same considerations are done in terms of pressure: with an enhancement of partial pressure for the product there will be a higher value of open circuit voltage.

The OCV is the value of the potential drop across the cell in case of ideal conditions: the only situation that satisfies this requirement is the open circuit condition, where the current is equal to zero. When the circuit is closed, the electrons start to flow into the external circuit, forming a current $I \neq 0$: the chemical equilibrium which was taking place at the electrodes is broken. The system is no more in the ideal conditions, but it is operating in the real conditions: this means that there will be some losses in terms of voltage drop across the cell. In case of a galvanic cell, the value of the potential drop will be lower and, with the same current, the produced

power will be lower; vice versa, in case of electrolytic cell, the voltage drop will be higher than the OCV value, requiring more power to make the reaction happen.

These differences between the real situation and the ideal one (OCV) occur because of the mass transport and charge transport phenomena.

To show the difference between real and ideal situation, a relation between current and potential is used: plotting the value of voltage drop across the cell as function of the current flowing in the external circuit, a clear characterization of the cell can be done. The curve obtained in this way is called polarization curve ($V = V(I)$). The same curve can be obtained as relation of voltage and current density V and i . The current density is equal to the ratio between current and cell's surface:

$$i = \frac{I}{Surface} \left[\frac{A}{m^2} \right] \quad (3.39)$$

because it is an easier way to express the current intensity.

The following plot was obtained using data coming from a microbial fuel cell tested during a laboratory experience at Politecnico di Torino.

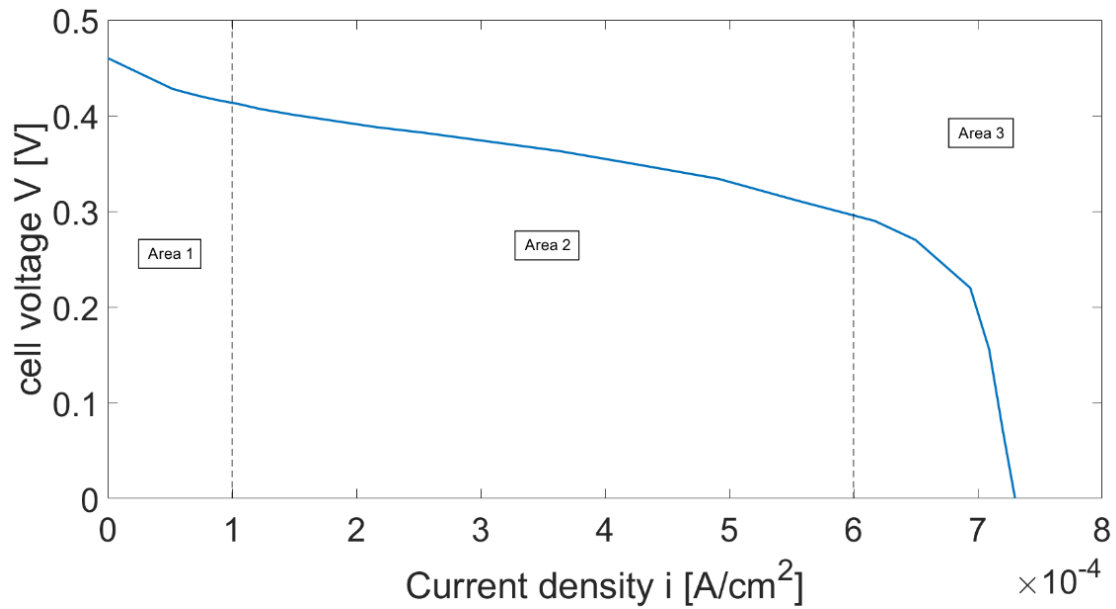


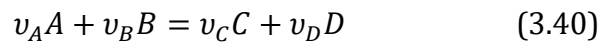
Figure 9 Polarization curve obtained from a Microbial Fuel Cell tested at Politecnico di Torino and used here as example

The graph can be divided in three different areas where there are different types of losses. In the first part of the graph (area 1) there are problems in the charge transfer related to the kinetic behaviour of electrochemical reaction both at the anode and at the cathode. In the central part of the curve (area 2) the losses appear due to the charge conduction related to ions conduction in the electrolyte and electrons conduction in the electrodes and the external circuit. The final behaviour of the curve (area 3) shows problems with mass transport related to molecules diffusion through the electrodes.

In the following section of this work, an analysis of these three different losses are done.

3.4.1 Charge transfer

This is the kinetic process related to the activation of the electrochemical reaction at the electrodes. The reaction takes place as two different half electrochemical reactions that occur separately at anode and cathode. These two electrodes have different kinetic, that is strictly related to the rate of reaction R . The rate of reaction for a generic reaction:



is defined as:

$$\begin{aligned} R &= -\frac{1}{v_A} \cdot \frac{dC_A}{dt} = -\frac{1}{v_B} \cdot \frac{dC_B}{dt} = -\frac{1}{v_C} \cdot \frac{dC_C}{dt} \\ &= -\frac{1}{v_D} \cdot \frac{dC_D}{dt} \end{aligned} \quad (3.41)$$

where C_i is the concentration of chemical species expressed in $\left[\frac{\text{mol}}{\text{m}^3}\right]$.

Differently from normal chemical reaction, for which the rate of reaction is only function of temperature, in case of an electrochemical reaction is given as function of both temperature and potential gradient in the electrodes η .

$$R = R(T, \eta) = k(T) \cdot e^{\frac{\alpha F}{RT} v_i z_i \eta} \quad (3.42)$$

where $k(T)$ is the constant rate that takes into account the effect of temperature on the activation energy;

F is the Faraday's constant;

ν_i is the stoichiometric coefficient of specie " i ";

z_i is the charge number of specie " i ";

η is the potential drop in the electrodes;

α is the transfer coefficient function of a symmetry factor β and the number of electrons transferred during the rate determining step of the reaction.

According to (3.41) an enhancement of the potential drop will increase the rate of the reaction: this means an enhancement of the kinetic.

This behaviour can be explained because the potential drop does not modify the activation energy directly as a catalyst, it modifies the energy level of both reactants and products. The symmetry factor β divides the effect of η between reactants and products.

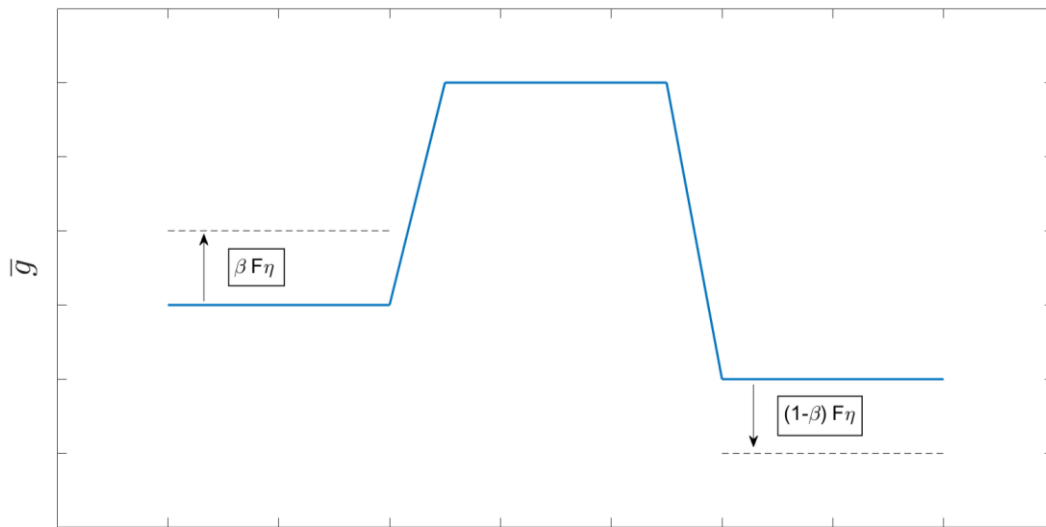


Figure 10 Energy amount before (left), during (centre) and after (right) a chemical reaction; the potential gradient do not modify directly the activation energy, but modifies the energy level with an increment for the reactants and a decrement for products

The relation used to consider the relation between voltage drop η and the current density i is the Butler – Volter equation:

$$i = i_0 \left[e^{\frac{\beta F}{RT} \eta_{act}} - e^{-\frac{(1-\beta)F}{RT} \eta_{act}} \right] \quad (3.43)$$

Where η_{act} is the activation overvoltage, the voltage drop used in order to activate the electrochemical reaction increasing the rate of reaction R ;

i_0 is the exchange current density, the current density exchanged during the electrochemical reaction when this one is in equilibrium.

By reversing the Butler – Volter equation, it is possible to obtain an expression of activation overvoltage as function of current density:

$$\eta_{act} = \eta_{act}(i) \quad (3.44)$$

A higher value of exchange current density means more easily the reaction can be activated. It depends on the length of three-phase boundary and other parameters (quantity, nanostructure and temperature of catalyst). The length of three-phase boundary is a parameter that takes into account the surface over which the reaction occurs. In the case of oxidation of hydrogen:



three different zones are required to make the reaction happens: porous phase, where the molecules of reactants (H_2) are fed; ionic phase that allows to remove the ions (H^+) from the point of the reaction; electronic phase that allows to remove the electrons (e^-) from the point of the reaction. These three phases coexist in the three-phase boundary (TPB).

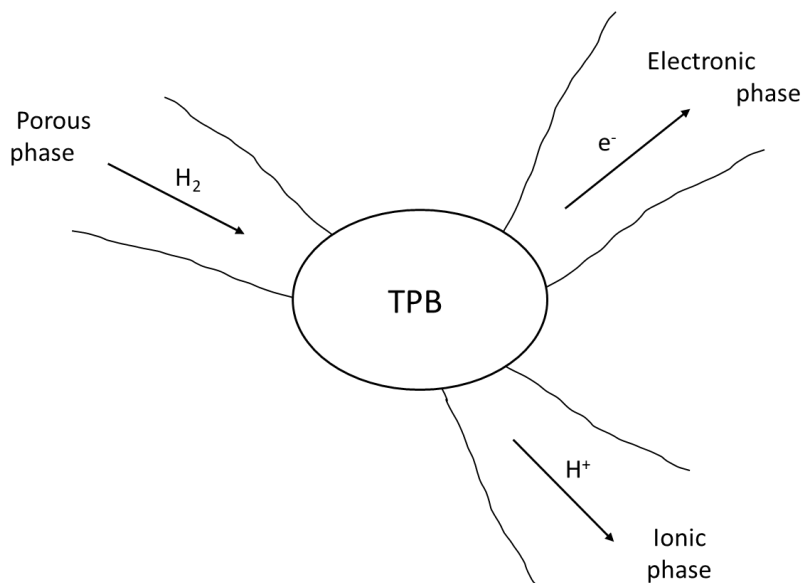


Figure 11 Scheme of three phase boundary

Considering a line merging all the TPBs, the length of TPB is obtained (l_{TPB}). A higher value of length of three-phase boundary corresponds to a larger area where the reaction can occur: this can be translated into a larger exchange current density i_0 .

3.4.2 Charge conduction

The central area of polarization curve shows the losses caused by transport phenomena of ions and electrons. The ionic conduction will give problems in the electrolyte while the electrons conduction will give problems in the external circuit. The ohmic drop can be evaluated as:

$$\Delta V_{ohm} = R \cdot I \quad (3.46)$$

$$\Delta V_{ohm} = \rho \cdot \frac{L}{A} \cdot I \quad (3.47)$$

where ρ is the resistivity of the material [$\Omega \cdot m$];

L is the length;

A is the surface.

It is clear that:

$$\Delta V_{ohm} \propto \rho \quad (3.48)$$

The resistivity can be expressed as the opposite of the conductivity of a material:

$$\rho = \frac{1}{\sigma} \quad (3.49)$$

That leads to the following correlation between voltage drop and conductivity:

$$\Delta V_{ohm} \propto \frac{1}{\sigma} \quad (3.50)$$

Considering both ion and electric conductivity (σ_{ion} and σ_{e^-}), the value of the first one has a so much lower value respect the second one:

$$\sigma_{ion} \ll \sigma_{e^-} \quad (3.51)$$

Considering the (3.29), it becomes clear that most of ohmic voltage drop is associated to the ions conduction across the electrolyte:

$$\Delta V_{ohm,ion} \gg \Delta V_{ohm,e^-} \quad (3.52)$$

This is explained knowing that it is easier for the electrons to flow into the external circuit respect for the ions to flow across the electrolyte.

As consequence, only the ohmic voltage drop caused by the ions transport is considered.

The ohmic overvoltage is expressed as follows:

$$\eta_{ohm} = R \cdot I \quad (3.53)$$

Knowing that:

$$R = \rho \cdot \frac{L}{A} \quad (3.54)$$

The ohmic overvoltage becomes:

$$\eta_{ohm} = \rho \cdot \frac{L}{A} \cdot I \quad (3.55)$$

But the current can be expressed as the product between the current density and the surface:

$$I = i \cdot A \quad (3.56)$$

Using the (3.55) and (3.56) and simplifying, the final expression for the ohmic overvoltage is deduced:

$$\eta_{ohm} = \rho \cdot \frac{L}{A} \cdot i \cdot A = \rho \cdot i \cdot L \quad (3.57)$$

The product between the resistivity and the surface can be incorporated in one single term called Area Specific Resistance (ASR), so the ohmic overvoltage becomes:

$$\eta_{ohm} = ASR \cdot i \quad (3.58)$$

Again, the voltage drop is function of current density.

Particular attention has to be done speaking about the length L : this is the length of the pathway done by the charged species (ions) and it can be assumed equal to the thickness of the electrolytic layer. Since the η_{ohm} is directly dependent on this term, L should be reduced as much as possible, always keeping enough thickness to ensure the insulation from electrons, that, in case of movement from one electrode to the other, would cause a short circuit.

3.4.3 Mass transport

At higher value of current density, corresponding to the last area of polarization curve, molecular diffusion losses are related. Molecular diffusion processes strictly affect the quantities of reactants achieving the three-phase boundary where the reaction occurs. The reactant concentration C_{react} is determined by the diffusive process thanks to which the fuel molecules are diffused across the electrodes. The diffuse process is strictly related to the diffusive coefficient that for a specie “ j ” is expressed as:

$$D_j^{eff} = \left(\frac{\varepsilon}{\tau}\right)^n \cdot D_j \quad (3.59)$$

where D_j^{eff} is the effective diffusion coefficient of specie “j” in the electrode;

D_j is the diffuse coefficient specie “j” at bulk conditions;

ε is the porosity;

τ is the tortuosity;

n is a fitting type parameter;

The porosity and the tortuosity are properties of porous layer: for a given porosity there are different configuration for a possible pathway, each with different tortuosity.

When there is a high value of current that has to be delivered, the number of reactions happening in the reaction point (TPB) increases as well. In this situation, the diffusion mechanism that should allow all the molecules to participate to the reaction can be too slow to replace quickly enough the molecules which have already reacted with new ones. This takes to a reactant concentration drop in the reaction point, which creates a potential drop η_{diff} . This mechanism happens both in the anode and in the cathode. Physically, the diffusion phenomena is not directly driving the potential drop, but it drives a reduction of the reactant concentration that will drive to a reduction of possible reaction that can happen in the reaction point TPB. In order to take the diffusion losses into account, the potential across the electrodes is evaluated at bulk conditions and then, with the help of a diffusion model, a value for η_{diff} is approximated. Possible models used for this evaluation are Fick law, Stefan-Maxwell model, Dusty gases model.

3.4.4 Polarization curve

Using all this information, an expression for the polarization curve is gained: this relation puts together the value of open circuit voltage OCV and, according to the value of the current density, gives a value for the potential modified by the three types of overpotential losses seen before.

The final relation expresses the relation between the potential across the electrodes V_c and the current density flowing through the cell. Since the open circuit voltage is function of temperature and pressure, also the potential V_c is a function of the same parameters plus the current density coming from the overpotential losses.

The expression is equal to:

$$V_c(T, P, i) = OCV(T, P) \pm \eta_{act}(i) \pm \eta_{ohm}(i) \pm \eta_{diff}(i) \quad (3.60)$$

Since the activation and the diffusion processes take place both in the anode and in the cathode, η_{act} and η_{diff} has to be considered for the two different electrodes.

The relation becomes:

$$V_c(T, P, i) = OCV(T, P) \pm \eta_{act,AN}(i) \pm \eta_{act,CATH}(i) \pm \eta_{ohm}(i) \pm \eta_{diff,AN}(i) \pm \eta_{diff,CATH}(i) \quad (3.61)$$

The expression written in this way is valid both for galvanic cells and electrolytic cell: in case of the first one the overpotentials are negative, which means the real value of the potential V_c has a lower value respect the open circuit voltage OCV. As consequence, the producible power $P = V_c \cdot I$ is lower than the ideal one. In case of an electrolytic cell, the overpotentials have a positive sign, which adds the losses to the OCV: this is translated in a higher voltage with the same current and a higher power required to make the reaction happen.

3.5 Thermal flux management

A particular interest has to be given to the heat production and management in an electrochemical cell. During the operations many thermal fluxes are exchanged. The heat is generated from two different contributions: the thermodynamics of the electrochemical reaction which takes an entropy modification: this is the reversible contribution to the heat flux. The other contribution considers the transport phenomena inside the cell, generating an irreversible contribution. Considering a galvanic cell, where $\Delta\bar{g} < 0$, the thermodynamic contribution is related to the entropy change in the electrochemical reaction:

$$\Phi_{rev} = T \frac{dS_{react}}{dt} \quad (3.62)$$

The entropy variation can be both positive or negative depending on the working mode of the cell: the thermal flux generated by this term can be positive or negative as well.

The heat flux produced by the reaction Φ_{react} corresponds to the reversible heat Φ_{rev} . Starting from the heat of the reaction:

$$\bar{q}_{react} = T \cdot \Delta\bar{s}_{react} \quad (3.63)$$

evaluated in $\left[\frac{J}{mol}\right]$, it is possible to multiply by the molar flow of fuel \dot{n}_{fuel} to obtain an expression for the thermal flux:

$$\Phi_{rev} = \Phi_{react} = \bar{q}_{react} \cdot \dot{n}_{fuel} \quad (3.64)$$

The term \dot{n}_{fuel} can be expressed in another way using the (3.22), while, exploiting the (3.62) to write the molar heat, the expression of reversible thermal flux becomes:

$$\begin{aligned} \Phi_{rev} = \Phi_{react} &= \bar{q}_{react} \cdot \dot{n}_{fuel} & (3.65) \\ &= T \cdot \Delta\bar{s}_{react} \cdot \frac{I}{z_{fuel} \cdot F} \end{aligned}$$

All the terms are positive except for the entropy variation that is negative, making the sign of the thermal flux negative: the reaction is exothermic.

$$|\Phi_{rev}| = -T \cdot \Delta \bar{s}_{react} \cdot \frac{I}{z_{fuel} \cdot F} \quad (3.66)$$

The irreversible contribution is related to the transport phenomena happening inside the cell. For example, the ohmic drop generates a heat flux for the joule effect:

$$\Phi_{ohm} = \eta_{ohm} \cdot I \quad (3.67)$$

It is possible to generalize for all the transport phenomena caused by the overpotentials and obtain:

$$\Phi_{irr} = I \cdot \sum_{j=1}^3 \eta_j \quad (3.68)$$

According to these considerations, the heat management is different from galvanic cell to electrolytic cell. In case of a galvanic cell, there are only heat generating phenomena: the cell will be always characterised by an exothermic behaviour. The generated heat flux is equal to the sum of reversible and irreversible terms:

$$|\Phi_{th}| = |\Phi_{rev}| + |\Phi_{irr}| \quad (3.69)$$

where Φ_{th} is the heat flux exchanged inside the cell and all the terms, in this case, are positive.

Making explicit the terms of the equation (3.69), it becomes:

$$\Phi_{th} = -T \cdot \Delta \bar{s}_{react} \cdot \frac{I}{z_{fuel} \cdot F} + I \cdot \sum_{j=1}^3 \eta_j \quad (3.70)$$

That can be fixed to get the final expression for the thermal flux:

$$\Phi_{th} = \left(-\frac{T \cdot \Delta \bar{s}_{react}}{z_{fuel} \cdot F} + \sum_{j=1}^3 \eta_j \right) \cdot I \quad (3.71)$$

Knowing that:

$$\Delta \bar{g}_{react} = \Delta \bar{h}_{react} - T \cdot \Delta \bar{s}_{react} \quad (3.72)$$

$$T \cdot \Delta \bar{s}_{react} = \Delta \bar{h}_{react} - \Delta \bar{g}_{react} \quad (3.73)$$

the (1.72) becomes:

$$\Phi_{th} = \left(-\frac{\Delta \bar{h}_{react} - \Delta \bar{g}_{react}}{z_{fuel} \cdot F} + \sum_{j=1}^3 \eta_j \right) \cdot I \quad (3.74)$$

$$\Phi_{th} = \left[-\frac{\Delta \bar{h}_{react}}{z_{fuel} \cdot F} - \left(-\frac{\Delta \bar{g}_{react}}{z_{fuel} \cdot F} + \sum_{j=1}^3 \eta_j \right) \right] \cdot I \quad (3.75)$$

the term $-\frac{\Delta\bar{g}_{react}}{z_{fuel}\cdot F} + \sum_{j=1}^3 \eta_j$ corresponds to the voltage of the cell V_c , so the expression is:

$$\Phi_{th} = \left(-\frac{\Delta\bar{h}_{react}}{z_{fuel}\cdot F} - V_c \right) \cdot I \quad (3.76)$$

This equation can be visualized on the polarization curve and it is clear how the initial chemical energy is transformed into electrical work and thermal energy. Considering a completely ideal reaction, the entropy generation due to the reaction and the transport phenomena is null. In this case the voltage would be $-\frac{\Delta\bar{h}_{react}}{z_{fuel}\cdot F}$ and it would remain constant with different current density, since the relation $V_c = V_c(i)$ is no longer true, and the thermal generation is null.

$$V_c = -\frac{\Delta\bar{h}_{react}}{z_{fuel}\cdot F} \quad (3.77)$$

$$\Phi_{th} = 0 \quad (3.78)$$

In this way, all the chemical energy is converted into electrical energy.

The real situation, considering the open circuit voltage situation, the entropy generation caused by the transport phenomena is still null, while the entropy generation due to the reaction occurrence is not null anymore. The voltage would still remain constant because there is not a direct dependence from the current density, but there is heat generation that decreases the level of V_c .

$$V_c = OCV = -\frac{\Delta\bar{g}_{react}}{z_{fuel} \cdot F} \quad (3.79)$$

$$\begin{aligned} \Phi_{th} &= \left[-\frac{\Delta\bar{h}_{react}}{z_{fuel} \cdot F} - \left(-\frac{\Delta\bar{g}_{react}}{z_{fuel} \cdot F} \right) \right] \cdot I \quad (3.80) \\ &= -T \cdot \Delta\bar{s}_{react} \cdot \frac{I}{z_{fuel} \cdot F} \\ &= -T \cdot \Delta\bar{s}_{react} \cdot \dot{n}_{fuel} \end{aligned}$$

In this case, part of chemical energy is converted into thermal energy while the other amount is completely used to generate electrical work.

The real reaction in closed circuit condition is the situation where the chemical energy is transformed into thermal energy, electrical work and losses due to transport phenomena. The entropy generation, both cause by the reaction and the transport phenomena, is not null. The voltage is given by the polarization curve equation and the thermal energy is equal to the amount given by the (3.82).

$$V_c = OCV - \eta_{act}(i) - \eta_{ohm}(i) - \eta_{diff}(i) \quad (3.81)$$

$$\Phi_{th} = \left(-\frac{\Delta\bar{h}_{react}}{z_{fuel} \cdot F} - V_c \right) \cdot I \quad (3.82)$$

Observing the polarisation curve and all these considerations, it is clear how increasing the current, there is a decrement of the voltage, higher the current, lower the voltage and higher the thermal energy production.

The considerations are different for an electrolytic cell, where $\Delta\bar{g} > 0$: the system can work in endothermic or exothermic behaviour depending on the entity of the thermal fluxes. In this case the thermal flux is equal to the difference between the heat flux generated by the reaction and the heat flux generated by the irreversibility:

$$|\Phi_{th}| = |\Phi_{rev}| - |\Phi_{irr}| \quad (3.83)$$

The heat flux produced by the thermodynamic irreversibility is evaluated in the same way as before except for the sign of entropy of the reaction that now is positive:

$$\Phi_{rev} = T \cdot \Delta\bar{s}_{react} \cdot \frac{I}{z_{fuel} \cdot F} \quad (3.84)$$

$$|\Phi_{rev}| = T \cdot \Delta\bar{s}_{react} \cdot \frac{I}{z_{fuel} \cdot F} \quad (3.85)$$

The heat flux produced by the transport phenomena irreversibility is the same as the galvanic cell:

$$|\Phi_{irr}| = I \cdot \sum_{j=1}^3 \eta_j \quad (3.86)$$

Substituting the equation (3.84) and (3.85), the thermal flux is obtained as before:

$$|\Phi_{th}| = |\Phi_{rev}| - |\Phi_{irr}| \quad (3.87)$$

$$= T \cdot \Delta \bar{s}_{react} \cdot \frac{I}{z_{fuel} \cdot F} - I \cdot \sum_{j=1}^3 \eta_j$$

$$\Phi_{th} = \left(+ \frac{T \cdot \Delta \bar{s}_{react}}{z_{fuel} \cdot F} - \sum_{j=1}^3 \eta_j \right) \cdot I \quad (3.88)$$

$$\Phi_{th} = \left(\frac{\Delta \bar{h}_{react} - \Delta \bar{g}_{react}}{z_{fuel} \cdot F} - \sum_{j=1}^3 \eta_j \right) \cdot I \quad (3.89)$$

$$\Phi_{th} = \left[\frac{\Delta \bar{h}_{react}}{z_{fuel} \cdot F} - \left(\frac{\Delta \bar{g}_{react}}{z_{fuel} \cdot F} + \sum_{j=1}^3 \eta_j \right) \right] \cdot I \quad (3.90)$$

$$\Phi_{th} = \left(\frac{\Delta \bar{h}_{react}}{z_{fuel} \cdot F} - V_c \right) \cdot I \quad (3.91)$$

Three possible situations can be analysed. If $\frac{\Delta \bar{h}_{react}}{z_{fuel} \cdot F} > V_c$ the thermal flux is larger than zero and the system will produce heat with an endothermic behaviour: the cell

needs heat to complete the reaction because the produced one will not be enough.

If $\frac{\Delta \bar{h}_{react}}{z_{fuel} \cdot F} < V_c$ the thermal flux is less than zero and the system will require thermal energy removal in order not to increase too much the temperature; the system will work with an exothermal behaviour. There is a point where the two contributions are the same, $\frac{\Delta \bar{h}_{react}}{z_{fuel} \cdot F} = V_c$: this point is called thermo neutral point and the voltage becomes the V_{TN} that makes the thermal flux exchanged by the electrolytic cell equal to zero.

3.6 High temperature solid oxide fuel cells (SOFC)

Fuel cells are open electrochemical system working in a galvanic regime where the chemical species as H₂ (fuel) are making react in order to produce electricity. As said before the difference in terms of Gibbs free energy is lower than zero, therefore the reaction happens spontaneously. As said in the introduction, fuel cells can be divided into different categories according to the materials and the operating temperature. In this study, only solid fuel oxide cells were mentioned due to the fact that all the tests and analysis were made on SOFC samples.

High temperature solid oxide cells offer several potential advantages: reversible electrode reactions, low internal resistance, high tolerance to typical catalyst poisons, production of high-quality waste heat for (among other uses) reformation of hydrocarbon fuels, as well as the possibility of utilizing hydrocarbon fuels directly.

They are different from other kind of cells (Molten salt fuel cells MSFC, phosphoric acid fuel cells PAFC, proton exchange membrane fuel cells PEMFC, alkaline fuel cells AFC, direct methanol fuel cells DMFC) because of the electrolyte material, that in this case is a solid layer made by a ceramic material, the ions conductivity, that becomes acceptable at higher temperature (600 – 700 °C), the operation mode, that could be fuel cell (FC) mode or electrolytic cell mode (EC). In this section solid oxide fuel cell (solid oxide cell in fuel cell mode) will be analysed.

A remind of structure and composition of the three layers of a SOFC has been reported here.

3.6.1 Cathode material

The cathode is the essential component in the solid oxide fuel cell in which the air enters the system and the oxygen is reduced using the electrons coming from the external circuit:



The reduction takes place at the three phases boundary (TPB) that involves the porous phase where the chemical specie which has to be reduced can arrive, the electronic phase where the electric charges can pass through, the ionic phase where the ions can move out. Considering the need of these three different phases, the material has been selected. Cathode material for SOFCs has to show high electrical conductivity, high catalytic activity for oxygen reduction. Most efficient cathode is usually constructed from a Mixed Ionic and Electronic Conductor

(MIEC) material. Nowadays there is a more interest in perovskite-structured oxides. With a lattice structure ABO_3 , this is a MIEC material which consists of three elements: the large cations A^{n+} , the small cations $B^{(6-n)+}$ and the oxide ions O^{2-} , where n is the positive charge on the A ions. [11] A sites occupy the vertex of the cube, B site occupies the centre of the cube and O sites occupy the centre of each face. The perovskite-type oxides have important application in SOFCs: this because the total charge on A and B (+6) can be achieved by different combination, 1 + 5, 2 + 4, 3 + 3 and also in more complex way [11] [12]. The ideal structure of perovskite is cubic: for the geometry of the structure, the following relation between radii of A, B and O ions can be written.

$$r_A + r_O = \sqrt{2}(r_B + r_O) \quad (3.93)$$

Due to ions that do not obey this relation and take to deformed variants of the ideal cubic structure, a tolerance factor t is introduced.

$$t = \frac{r_A + r_O}{\sqrt{2}(r_B + r_O)} \quad (3.94)$$

A tolerance factor t close to 1 means that the structure is close to the ideal one.

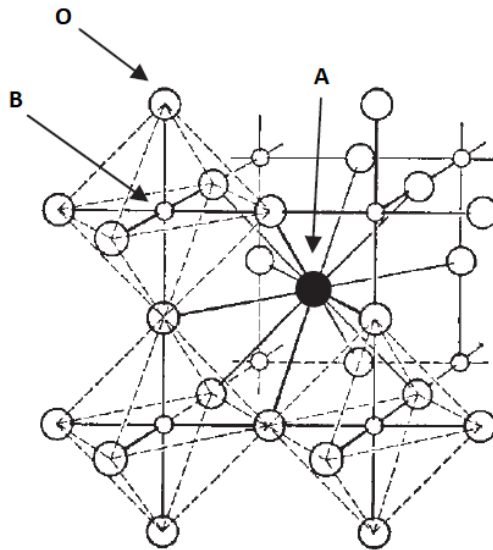


Figure 12 Ideal perovskite structure [4].

The high stability of crystal structure takes the perovskites to the possibility to accommodate a large amount of oxygen deficiency. Therefore, these types of structure show high electronic properties. Perovskite material are largely used as electrode material for fuel cell since there is a large number of dopants which can be used to dope the basic structure and increase the wanted properties.

The state of art for the solid oxide fuel cell includes materials as lanthanum strontium manganite (LSM) that operates at temperature in the range of 1000 °C: this temperature means large difficulties to manage the heat and problems with breaking down of the cell due to a too lower material resistance to heat. Material that can resist to this temperature will increase the system cost and complexity. On the other side, reducing the operating temperature, there will be an enhancement of the polarization resistance R_p that means higher losses. Therefore, the present research focusses the attention on different materials which exhibit similar value of

ionic and electronic conductivity at intermediate temperature, in the range of 600 – 800 °C [13].

3.6.2 Anode material

Like the cathode, the anode has to possess high catalytic activity for fuel oxidation and high electrical conductivity. The anode is usually constructed from cermet, a mixture of ceramic and metallic material, which works both as catalyst and electronic phase. At high temperature, the cermet has such good properties: activation of oxidation reaction, remarkable electrons conductivity and good porosity.

3.6.3 Electrolyte material

In a SOFC, the electrolyte layer must satisfy some characteristics in order to make good cells and must be dense and leak-tight; it must be able to make a thin layer to reduce ionic resistance.

The overvoltage caused by ohm effect is given by:

$$\eta_{ohm} = ASR \cdot i \quad (3.95)$$

The parameter *ASR* is equal to the product of two terms: the thickness of the electrolyte and the resistivity:

$$ASR = L \cdot \rho \quad (3.96)$$

A first way to reduce the area specific resistance, and on consequence the overvoltage, is to reduce the thickness of the electrolyte L . The other possible solution is to choose materials showing a lower resistivity ρ (or higher ionic conductivity σ).

There are two types of electrolytes: oxide conducting electrolytes and proton conducting electrolytes. Fluorite oxides like yttria-stabilized zirconia (YSZ) is the most popular oxide electrolyte in SOFCs development. This material has high conductivity of O^{2-} ions at high temperatures.

Gg-doped ceria (GDC) is another popular oxide ion conductor with high conductivity, but different from YSZ, GDC shows electronic conductivity under reducing environment. Nevertheless, there are other kinds of material whose oxide ion and proton conduction satisfy the requirement [11]. For instance, perovskite oxides of $LaGaO_3$ and $CaTiO_3$ (oxide ions), $BaCeO_3$ and $BaZrO_3$ (protons), perovskite-related oxide of $Ba_2In_2O_5$ (oxide ion), and the new crystal-phase oxides of La_2GeO_5 [14] are highly attractive for use as the electrolyte of SOFCs.

3.6.4 SOFC structure

Different types of SOFC have been developed in the past years and a first classification could be done considering the structure: anode supported SOFC, electrolyte supported SOFC, cathode supported SOFC. In these three different structures, the cell is made using one layer as support while the other two are thinner and built on the support layer. The samples used in this work were made using an electrolyte as support and painting the electrodes on it.

The anode supported SOFC is the best configuration because it offers the highest three phase boundary (TPB) where the fuel is oxidized (the anode).

The electrolyte layer is one of the major causes of ohmic drop: in the electrolyte supported SOFC, this could be a problem, rising up the losses; the electrolyte remains a robust structure but less efficient respect to the anode supported SOFC.

The cathode supported SOFC has problems with mass transport.

3.7 SOFC layers used in this study

Here there is a literature review about the materials used to build the samples for this work.

The electrode material used for the cathode was both lanthanum strontium cobalt ferrite (LSCF) and LSCF doped with erbium-stabilized bismuth (ESB). The anode was made by painting platinum ink on the electrolyte layer as reference electrode. The electrolyte material was gadolinium-doped ceria (GDC).

3.7.1 LSCF electrode

Electrodes for SOFCs must possess many properties such as high electrical conductivity and high ion conductivity: Mixed Ionic and Electronic Conductor (MIEC) is what satisfies the required characteristic.

In SOFCs manganite or cobaltite-based perovskite oxygen electrodes such as (LaSr)MnO_{3+δ} (LSM) and (LaSr)(CoFe)O_{3-δ} (LSCF) are the most investigated materials. LSCF perovskite oxide possesses a high oxygen vacancy concentration and ion mobility several orders of magnitude higher than LSM (oxygen ion conductivity of LSCF ~ 0.2 S cm⁻¹ at 900°C) and superior electrical conductivity (~250 S cm⁻¹ at 800°C) [15].

Most critical problem of LSCF is the Sr segregation at the interface between LSCF based electrodes and electrolytes. The enhancement of Sr quantity at the interface de-activate the reaction sites for oxygen reduction, consequently increasing the cathode polarization resistance.

A recent study by Shuai He et al. [16] showed that Sr segregation from LSCF can be reduced by using Nb-doped La_{0.6}Sr_{0.4}Co_{0.2}Fe_{0.7}Nb_{0.1}O_{3-δ} (LSCFNb) electrode with 40% Er_{0.4}Bi_{1.6}O₃ (ESB) composite electrode fabricated by decoration method and directly assembled on barrier-layer-free yttrium-stabilized zirconia (YSZ) electrolyte cells. Under cathodic polarization at 250 mA cm⁻² and 750 °C for 100 h, a very stable ESB-LSCFNb/YSZ interface was achieved. In the case of LSCFNb/YSZ cell, a significant Sr segregation and diffusion was observed on the electrolyte surface, while, using an ESB-LSCFNb/YSZ cell, the ESB decoration improves the electrocatalytic activity and stability of cathode [16].

3.7.2 Erbium stabilized Bismuth oxide (ESB)

Doped bismuth oxides have high value of ionic conductivity (0.023 S cm⁻¹ at 500 °C and 0.37 S cm⁻¹ at 700 °C), 1 or 2 orders of magnitude larger than yttria-stabilized zirconia (YSZ). This kind of oxide, such as ESB, possess optimal oxygen surface

exchange kinetics, but there are also some negative aspects, such as low melting point, high reactivity and phase instability in reducing atmosphere, that make these oxides not as utilized as oxygen ion conductors [16]. In this study ESB is applied to cobaltite-based perovskite cathode LSCF in order to show the formation of a layer between electrolyte and electrode after polarization.

3.7.3 Gadolinium-doped ceria (GDC)

Electrolyte layer was composed by GDC powder. Ceria-based electrolytes have been founded to possess the highest values of ionic conductivity and diffusion constant among a group of analysed fluorite oxide [17]. Ionic conductivity of gadolinia-stabilized ceria is about one order of magnitude larger than that of yttria-stabilized zirconia (YSZ) also reducing the operating temperature. The values of conductivity found in literature are $4.3 \cdot 10^{-2}$ for GDC and $1.8 \cdot 10^{-2}$ for YSZ at 700 °C; reducing the temperature up to 500 °C, the values become $5.9 \cdot 10^{-3}$ for GDC and $7.8 \cdot 10^{-3}$ for YSZ [18]. Gadolinium doped ceria electrolyte is one of the promising materials for electrolyte layer due to the higher specific surface area of nano-sized particles, which leads to faster densification and lower sintering temperature [19]. Ceria and rare earth-doped ceria powders have important application in solid oxide fuel cell. The dopants add oxygen vacancies in the anion sub-lattice: these vacancies are responsible for the high value of ionic conductivity of GDC observed before. A solid solution of GDC can be obtained with different techniques as conventional ceramic route or chemical methods. To obtain GDC samples with high densities by conventional sintering method, temperature in the order of magnitude of 1500 °C is required [20].

4. Methods

This study shows the performance improvement of LSCF+ESB cathode applied on GDC electrolyte. The GDC electrolyte was obtained by pressing the GDC powder while the cathode was synthesized using the starting chemicals through sol-gel method.

4.1 Synthesis of LSCF decorated with ESB

The same process described before for the work of Shuai He et al. [16] was used in this work to study the interface between LSCF+ESB cathode and GDC electrolyte. LSCF powder was synthesized by sol-gel method starting from the following chemicals: $\text{La}(\text{NO}_3)_3 \cdot \text{H}_2\text{O}$, $\text{Sr}(\text{NO}_3)_2$, $\text{Co}(\text{NO}_3)_2 \cdot \text{H}_2\text{O}$, $\text{Fe}(\text{NO}_3)_3 \cdot \text{H}_2\text{O}$. A quantity of 0.05 mole of powder was prepared using a ratio of 0.6 : 0.4 : 0.2 : 0.8 (La/Sr/Co/Fe). At these chemicals were added citric acid and ethylene diaminetetraacetic acid (EDTA) in a molar ratio of 2:2:4 (metal ions/EDTA/CA) and ammonia solution $28\% \text{NH}_3 \cdot \text{H}_2\text{O}$. The pH of the solution was adjusted to 7 and the solution was stirred on a hot plate until the dry gel was formed, then dried for 8 h at 150°C in an oven. The resultant

powder was calcined at 900 °C in air for 2 h with a ramp of 2 °C min⁻¹. The used quantities are shown in table A in the appendix section.

Er_{0.4}Bi_{1.6}O₃ (ESB)-decorated LSCF electrode powder was synthesized by solid - gel method. Two powders were prepared with different weight percentages: 40% ESB - 60% LSCF and 50% ESB - 50% LSCF. ESB aqueous precursor solution consisting of Er(NO₃)₃·5H₂O, Bi(NO₃)₃·5H₂O, EDTA, anhydrous citric acid, and ammonia was constantly stirred on a heating stage; then, LSCF powder was added to both ESB precursor solutions and stirred until the gelation starts. The resultant gels were further dried at 150 °C for 8 h in an oven and then calcined at 600 °C in air for 2 h with a ramp of 2 °C min⁻¹, forming ESB-decorated LSCF powder (ESB-LSCF). Table B in the appendix section shows the used values.

LSCF cathode with a composition 0.6 : 0.4 : 0.2 : 0.8 (La/Sr/Co/Fe) without adding ESB was prepared to allow the comparison between the presence or not of Erbium-stabilized Bismuth.

4.2 Sintering of GDC electrolyte pellet

Electrolyte pellets were synthesized by die-pressing 2 g of Gd_{0.1}Ce_{0.9}O_{1.95} (GDC) and sintering the pellets at 1450 °C for 5 h.

The pressing procedure was made by the pressing machine shows in figure 14: the weighted quantity of GDC was putted in a mould: the powder was inserted between two pellets and a punch was used to transmit the pressure. Then, the mould was putted on the working stage, the oil release valve was blocked, the pressure was

increased using the rocker, a value of 4 MPa was reached and maintained for more than 30 seconds.

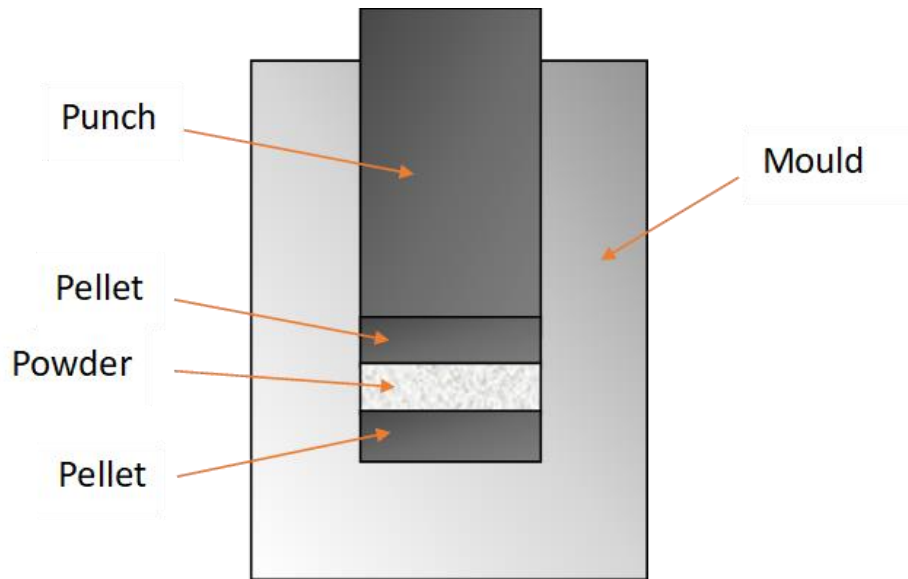


Figure 13 Schematic image of the mould used to press the powder of GDC

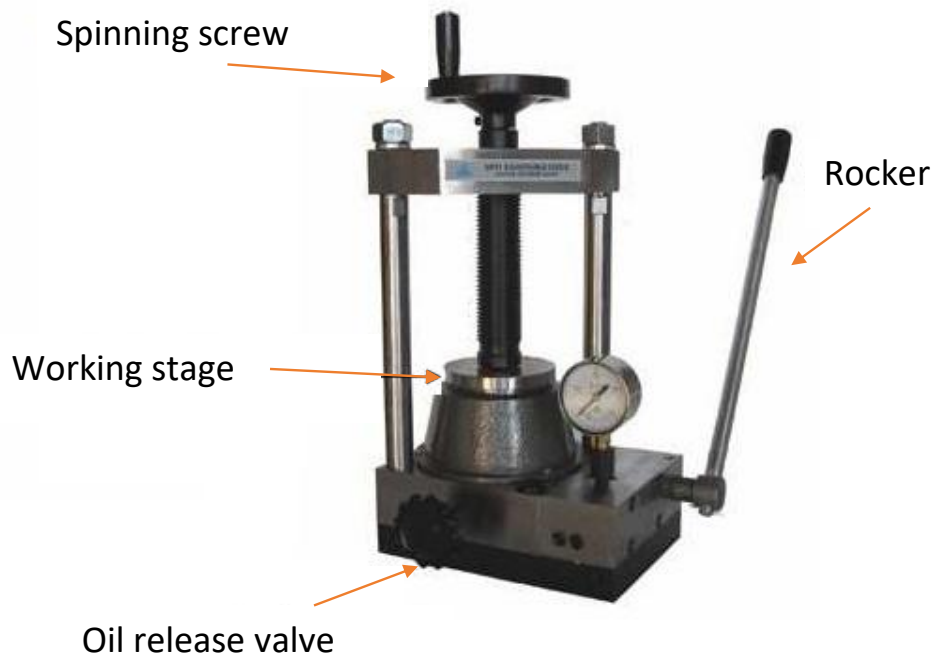


Figure 14 Pressing machine used to increment the pressure up to the requested one

A large number of cells was made: the main problem was to use a correct quantity of powder in order to obtain a cell without cracks or failure. The used amount was 2 g of GDC.

The as built cells were sintered in the furnace using a ram to reach the temperature in order to avoid brakes: ramp of 1 °C min⁻¹ up to 600 °C, 1 h at 600 °C, ramp of 2 °C min⁻¹ up to 1450 °C, 5 h at 1450 °C. After this procedure the number of broken cells was almost half of the starting one. The intact cells were taken and used in the following step.

4.3 Fabrication of direct assembled LSCF-ESB on GDC

Pt paste was painted on the centre and edge of the GDC electrolyte pellet and sintered at 1100 °C for 2 h with a ramp of 2 °C min⁻¹ as the counter and reference electrodes. As-synthesized LSCF-ESB powders were dispersed in an ink vehicle with a weight ratio of 7:3 and subsequently the cathode paste was painted and dried at 150 °C on the other side of the electrolyte symmetrically opposite to the Pt counter electrode. Pt mesh was painted and dried at 150 °C as current collector on LSCF-ESB cathode.

4.4 Electrochemical performance

The electrochemical impedance was measured by electrochemical spectroscopy impedance (EIS) [21] under open circuit condition in a range of 0.1Hz to 100 kHz with a signal amplitude of 20 mV. The shape and the position of the arches give information about ohmic resistance (R_{Ω}), electrode polarization resistance (R_p) and the causes of the losses: larger high frequency arch means high R_p in charge transfer while larger low frequency arch means high R_p associated with mass transport process. The evaluation of R_{Ω} and R_p was done with the intercepts of the arches with the x-axis: R_{Ω} was obtained with the intercept of high frequency arch, R_p was evaluated as difference between high and low frequency arch intercepts. The ohmic resistance corresponds to the resistance of the electrode, electrolyte and contact resistance between them, see Figure 15.

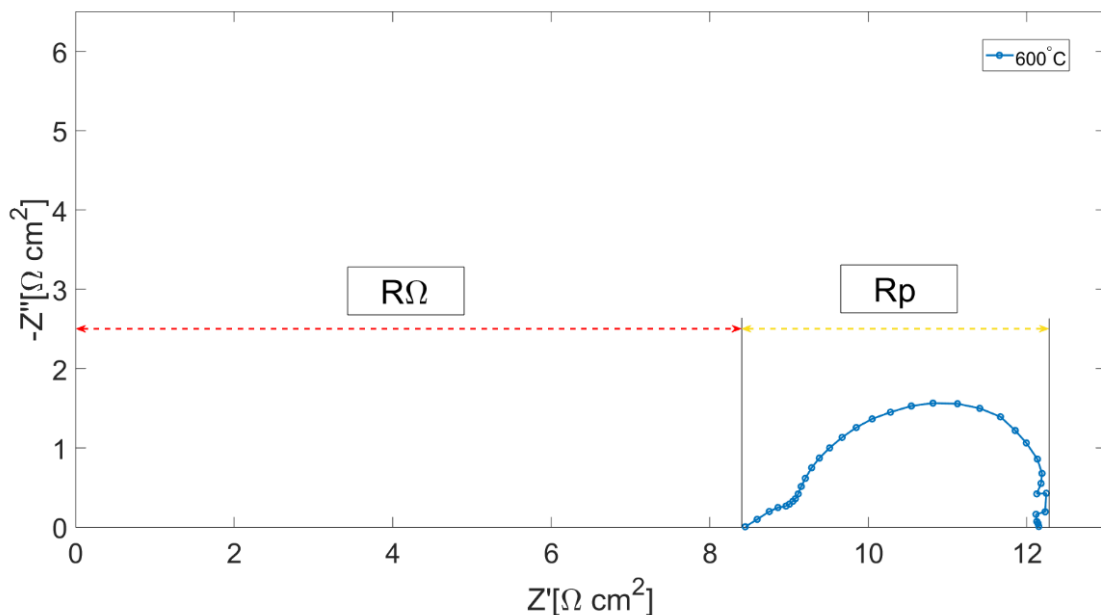


Figure 15 Electrochemical impedance spectroscopy, evaluation of R_p and R_{Ω}

The electrochemical tests were performed using the furnace showed in figure 16: the sample was put below the thinner ceramic tube. Platinum meshes were applied on the top and on the bottom of the cell in order to maximize the contact between electrodes and the electrical cables to collect the data.

Then, the furnace was closed and heated up to 750 °C with a ramp of 2 °C min⁻¹ not to break the cell with a too fast heating up. Data for the electrochemical impedance spectroscopy were collected at this temperature and then the furnace was cooled down to 600 °C with the same ramp, collecting data each 50 °C. After the EIS, the cell was heated up to 750 °C and polarized for 100 h with a cathodic current of 1000 mAcm⁻².



Figure 16 Furnace and test station used to measure the electrochemical properties of the sintered cells at different temperature



Figure 17 Particular of the furnace with the cell pressed between the two tubes in order to increment the electrons transfer

5. Results and discussion

The results show that there is a reduction in the ohmic resistance when ESB is added to LSCF. Here simple LSCF applied on GDC results first and then LSCF+ESB applied on GDC results are shown.

5.1 Impedance behaviour of LSCF cathode/GDC electrolyte

Figure 18 show the Electrochemical Impedance Spectroscopy (EIS) measured on the half-cell made by LSCF electrode directly assembled on the GDC electrolyte as explained above. At temperature of 600 °C, there is a clear separation of low and high frequency arcs, but with the increase of the temperature the impedance arcs decrease with a reduction of both R_p and R_Ω . This means the higher the temperature, the higher the performance of the cell.

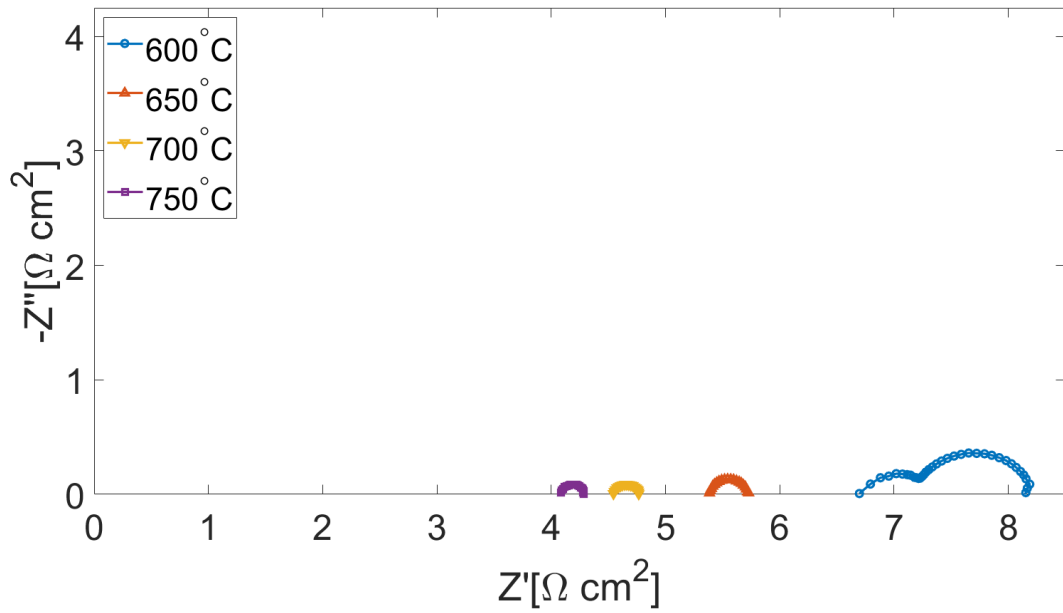


Figure 18 EIS of LSCF applied on GDC half-cell, sample A

Other three samples were tested and figures 19, 20 and 21 show the results: samples B and C have very good quality: the resistance possesses very low value at 700 °C already that means very high performance. Sample D has similar results compare with the considered sample A in figure 18. Unfortunately, these three cells broke down during the polarization and there are no further data available.

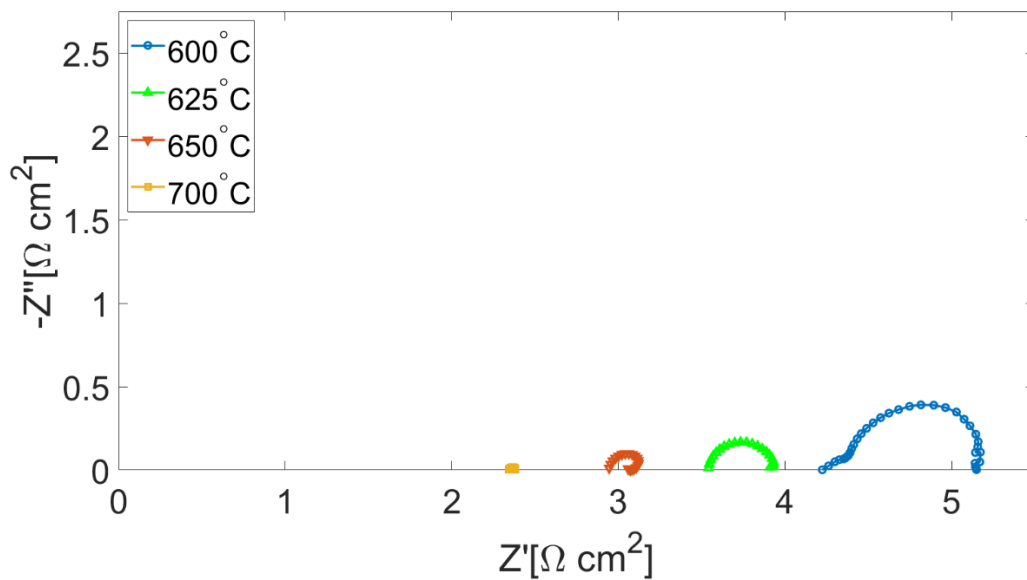


Figure 19 EIS of LSCF applied on GDC half-cell, sample B

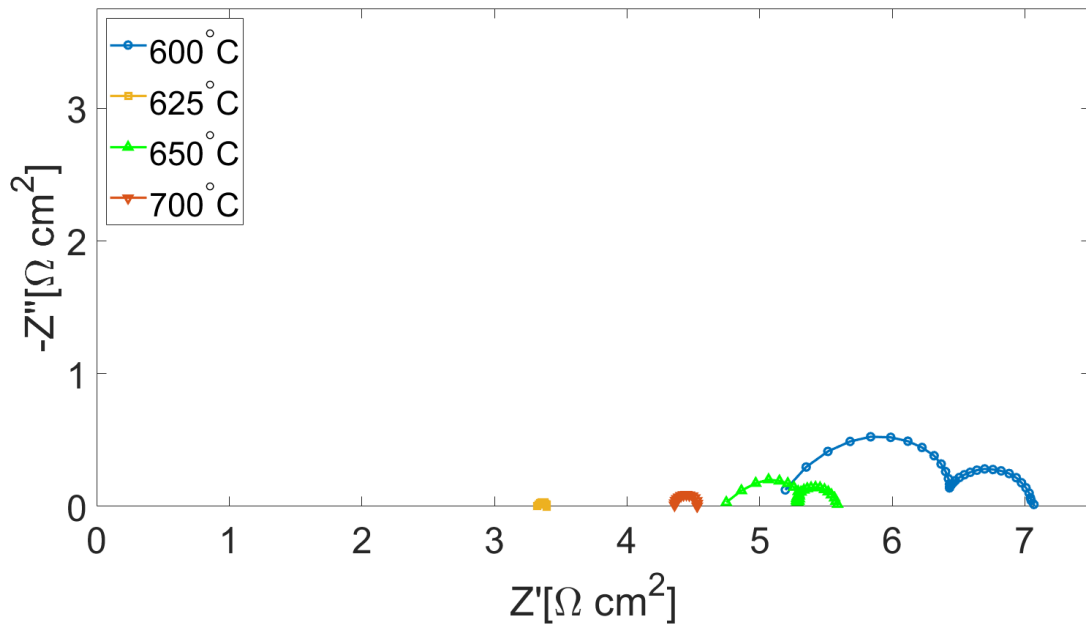


Figure 20 EIS of LSCF applied on GDC half-cell, sample C

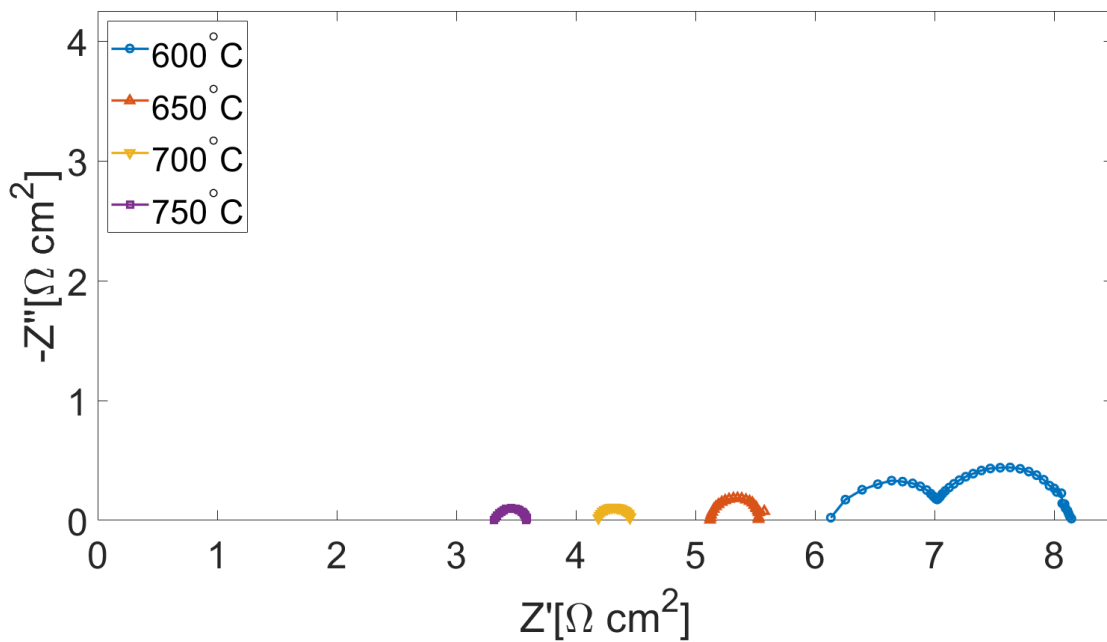


Figure 21 EIS of LSCF applied on GDC half-cell, sample D

The activation energy E_a for the reaction has been obtained using the Arrhenius Law:

$$\ln(k) = \ln(A) - \frac{E_a}{RT} \quad (5.1)$$

where k is the rate constant and in this case, it corresponds to R_p ; A is the pre-exponential factor or Arrhenius factor; R is the gas constant and T is the temperature. Figure 22 shows the activation energy plot of the reaction at the LSCF/GDC interface. From the slope, the activation energy is $\sim 116 \text{ kJmol}^{-1}$ for the oxygen reduction reaction. A larger slope of the fitting means a higher activation energy. If the activation energy, directly proportional to the slope, is higher, there will be a higher resistance at lower temperature. The aim of this work is to reduce the resistance also at a lower temperature.

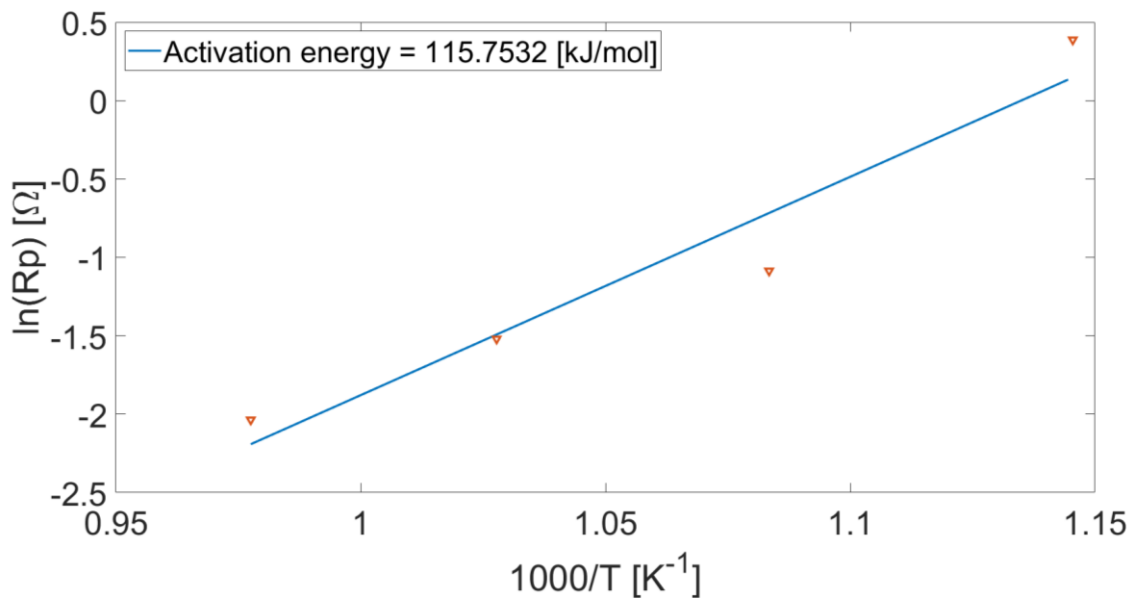


Figure 22 Activation energy of LSCF applied on GDC half-cell

Then the LSCF on GDC half-cell was polarized for 24 hours with a cathodic current of 1000 mAcm^{-2} at 750°C . The cathode potential decreases due to the reduction of the resistance under the polarization, as shown in the Figure 23.

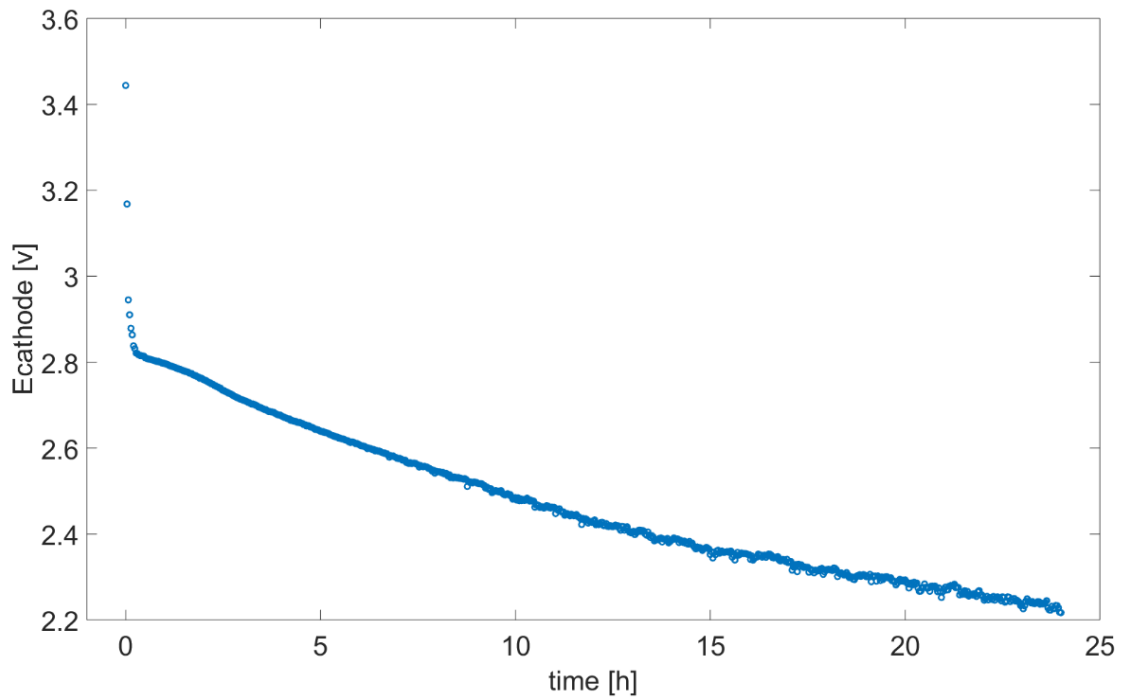


Figure 23 Polarization curve of LSCF applied on GDC half-cell under cathodic current of 1000 mAcm^{-2} at 750°C .

Figure 24 shows the impedance spectroscopy before and after 24 h polarization. As the GDC electrolyte thickness is close, it is possible to see the significant reduction of the ohmic resistance R_Ω , responsible for the reduction of E_{cathode} . On the other hand, the reduction in the electrode polarization resistance (i.e., the impedance arc) is relatively small before and after the cathodic polarization treatment. This indicates that the cathodic polarization mainly enhances the directly assembled LSCF/GDC interface by reducing the contact resistance between LSCF cathode and GDC electrolyte. This is consistent with previous studies of the directly assembled electrode/electrolyte interface induced by the cathodic polarization.

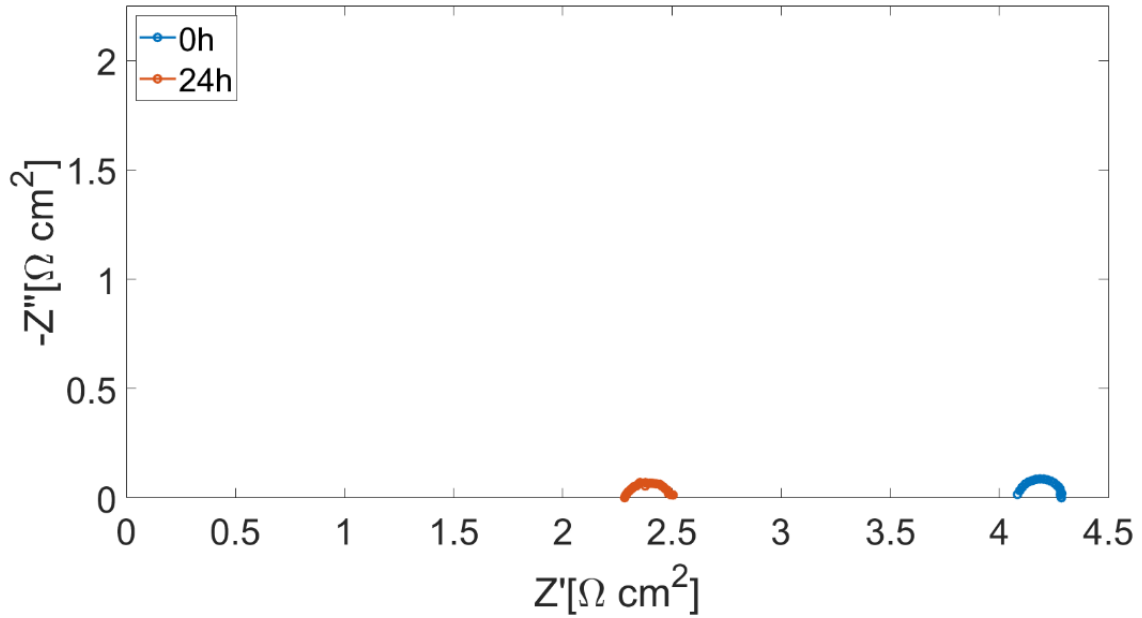


Figure 24 Effect of polarization at 750°C on LSCF applied on GDC half-cell

5.2 Impedance behaviour of LSCF-ESB cathode/GDC electrolyte

Similar tests were performed on the LSCF-ESB/GDC half-cell. The utilised ratios were 6 : 4 and 1 : 1 (LSCF/ESB). The sample were tested in the electrochemical impedance spectroscopy test station in order to measure the impedance at different temperature and obtain the energy activation. Figures 25 and 26 show the impedance plots of the cell measured at different temperatures for both the analysed ratios. Similar to that of LSCF/GDC cells, both R_{Ω} and R_p are reduced with increasing the temperature.

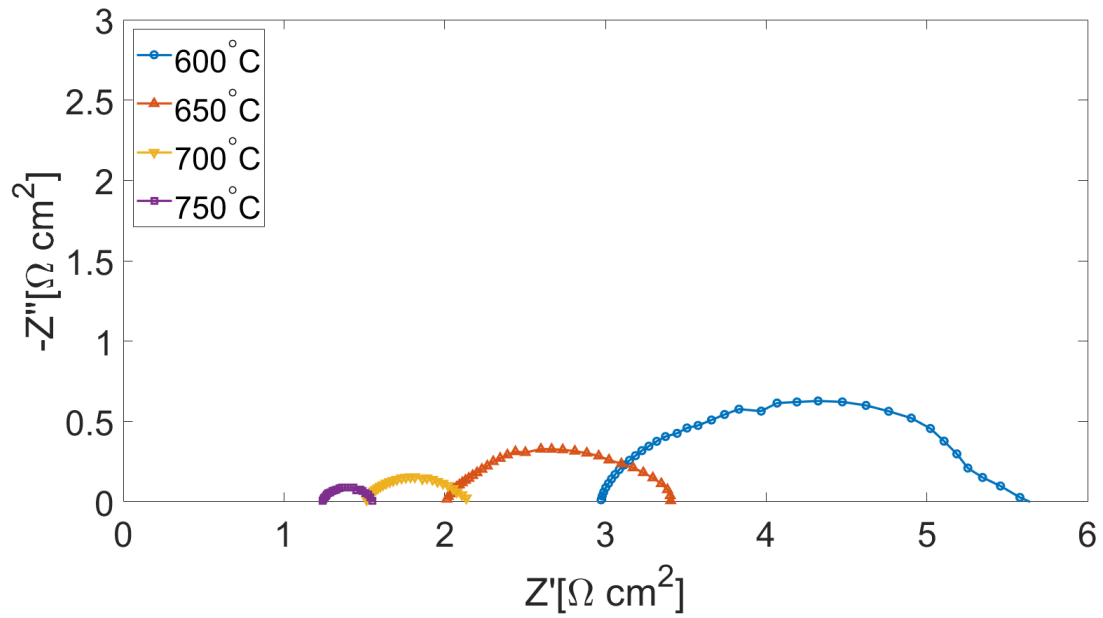


Figure 25 EIS of LSCF+ESB applied on GDC half-cell ratio 6 : 4 (LSCF/ESB)

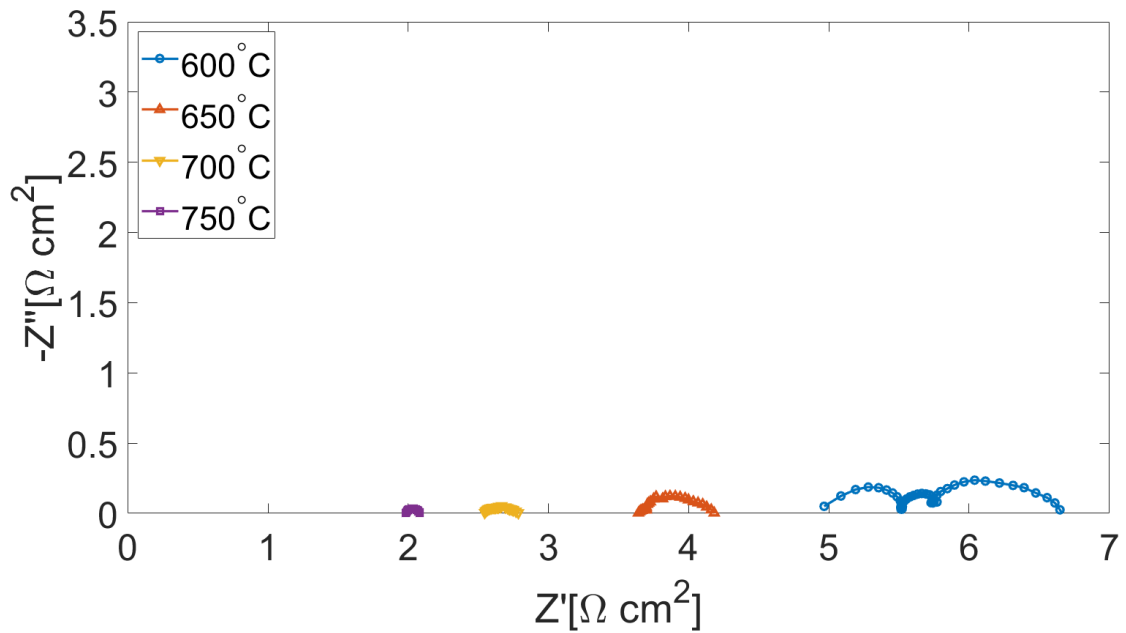


Figure 26 EIS of LSCF+ESB applied on GDC half-cell ratio 1 : 1 (LSCF/ESB)

Ratio 6 : 4 seems to possess a lower resistance both at higher and lower temperature: for this reason, the cell with this combination of components was chosen as sample for the further analysis.

The energy activation is $108 \left[\frac{\text{kJ}}{\text{mol}^{-1}} \right]$ (see Figure 27) and compatible with the values in literature. Its value is lower in comparison with LSCF on GDC half-cell: this means lower resistance at lower temperature.

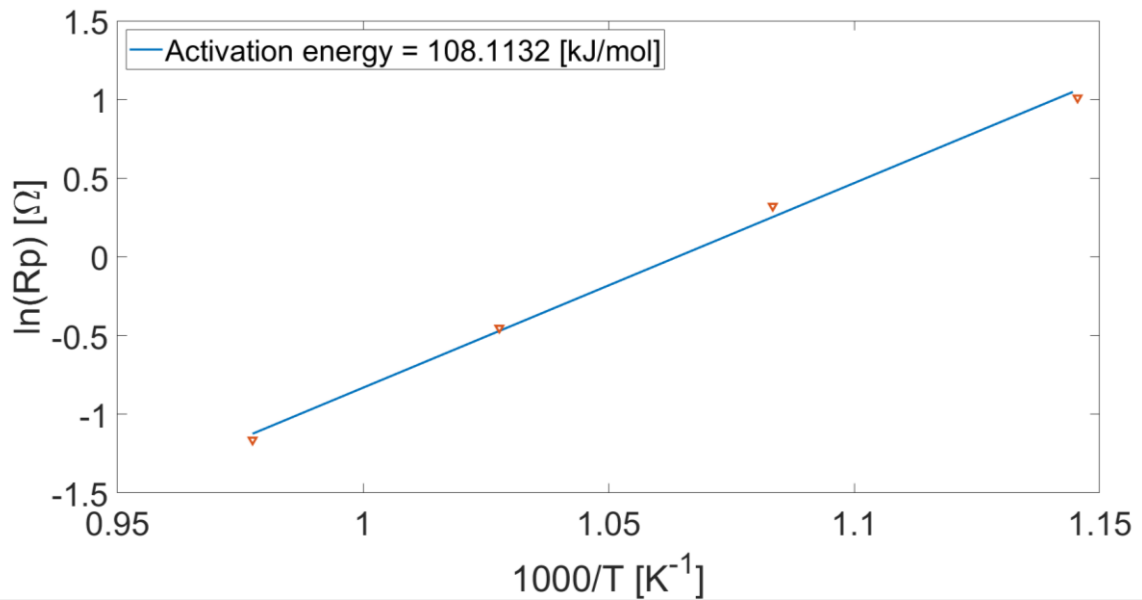


Figure 27 Activation energy of LSCF+ESB applied on GDC half-cell

The LSCF+ESB/GDC half-cell was also polarized with a cathodic current of 1000 mAcm^{-2} for 100 h at 750°C . The results show an initial enlargement of the cathode potential probably due to a transient phenomenon. However, there is a substantial reduction of E_{cathode} after 100 hours of polarization.

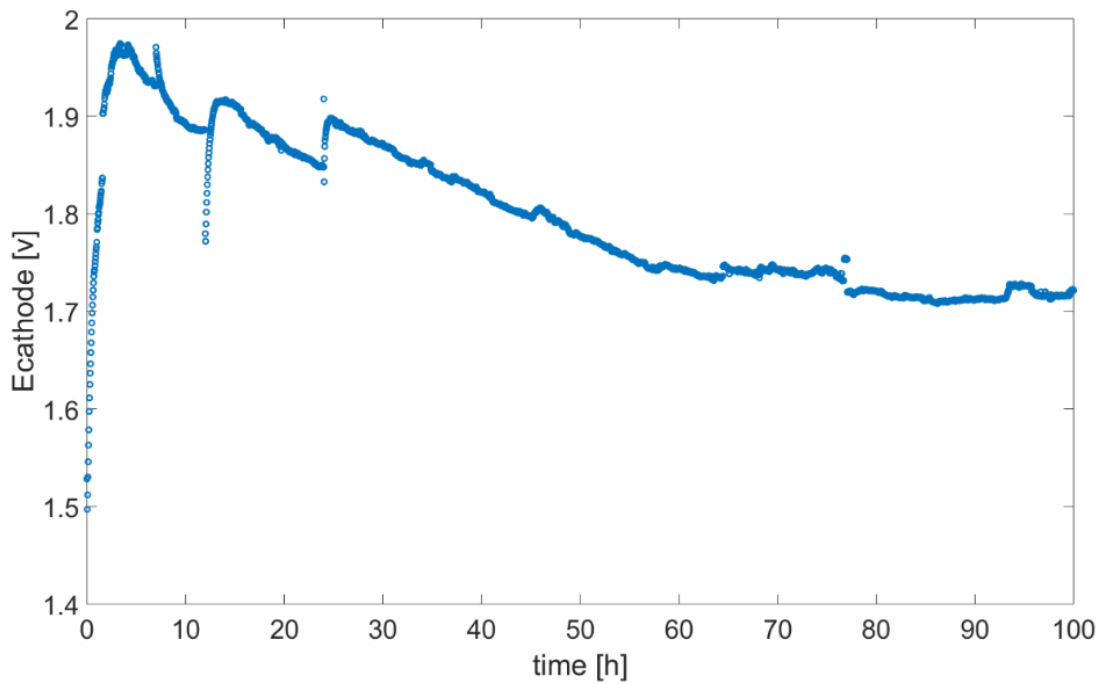


Figure 28 Polarization curve of LSCF+ESB applied on GDC half-cell under cathodic current of 1000 mAcm⁻² at 750°C.

Figure 29 and 30 compare the activation and polarization behaviour of LSCF-ESB/GDC and LSCF/GDC interface measured under identical polarization conditions. The results indicate the very different impedance and polarization performance of the ESB decorated LSCF and pristine LSCF cathodes on GDC electrolyte interface induced under cathodic polarization conditions. The different behaviour implies the very different interface microstructure induced by the cathodic polarization.

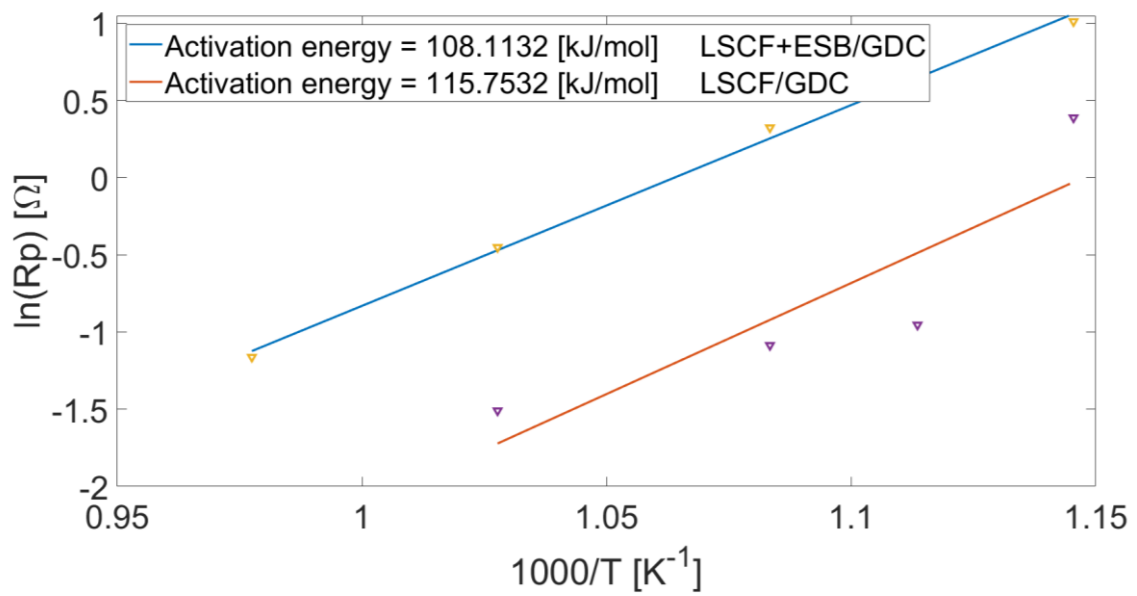


Figure 29 Activation energy of LSCF and LSCF+ESB applied on GDC half-cells

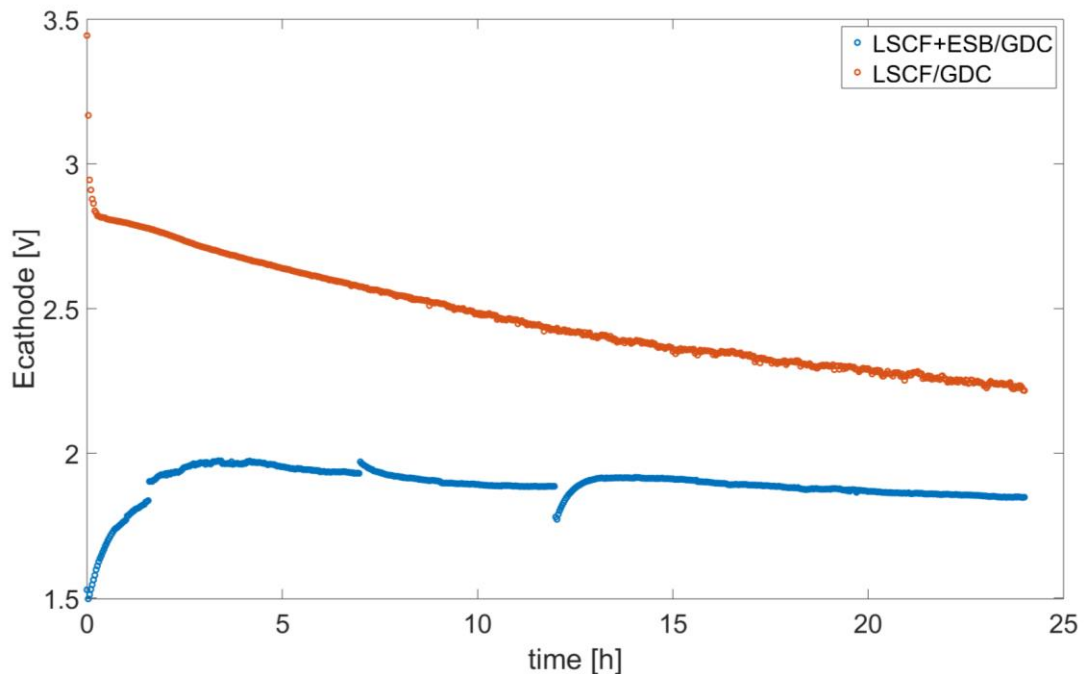


Figure 30 Polarization curve of LSCF and LSCF+ESB applied on GDC half-cells under cathodic current of 1000 mAcm^{-2} at 750°C .

Looking at the behaviour of E_{cathode} with the time, the combination of LSCF+ESB on GDC shows better performance at lower temperature, becoming suitable materials for the aim to reduce the operating temperature for solid oxide fuel cells.

5.3 Microstructure of electrode/electrolyte interface

The half-cell made by GDC and LSCF-ESB morphology was investigated using the Scanning Electron Microscopy (SEM) and the Transmission Electron Microscopy (TEM). The results show that there is a migration of ESB particles towards the interface zone after the polarization.

Figure 31 and 32 show the morphology of the interface between LSCF-ESB electrode and GDC electrolyte made by the adhesive tape peeling (figure 31) and acid treatment (figure 32).

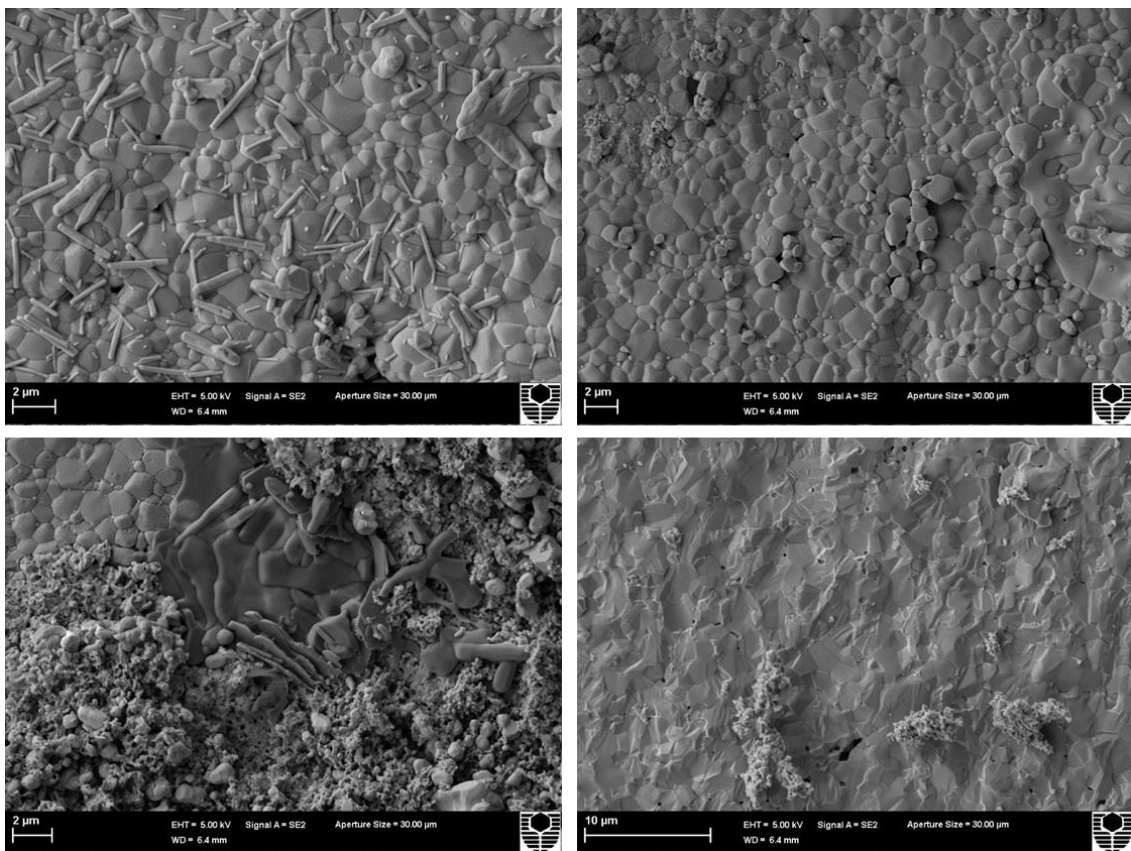


Figure 31 SEM images of LSCF-ESB applied on GDC after cathode removal through adhesive tape. A: needle shaped ESB particles on GDC substrate; B: GDC particles; C: irregular particles of LSCF; D: LSCF particles on GDC substrate

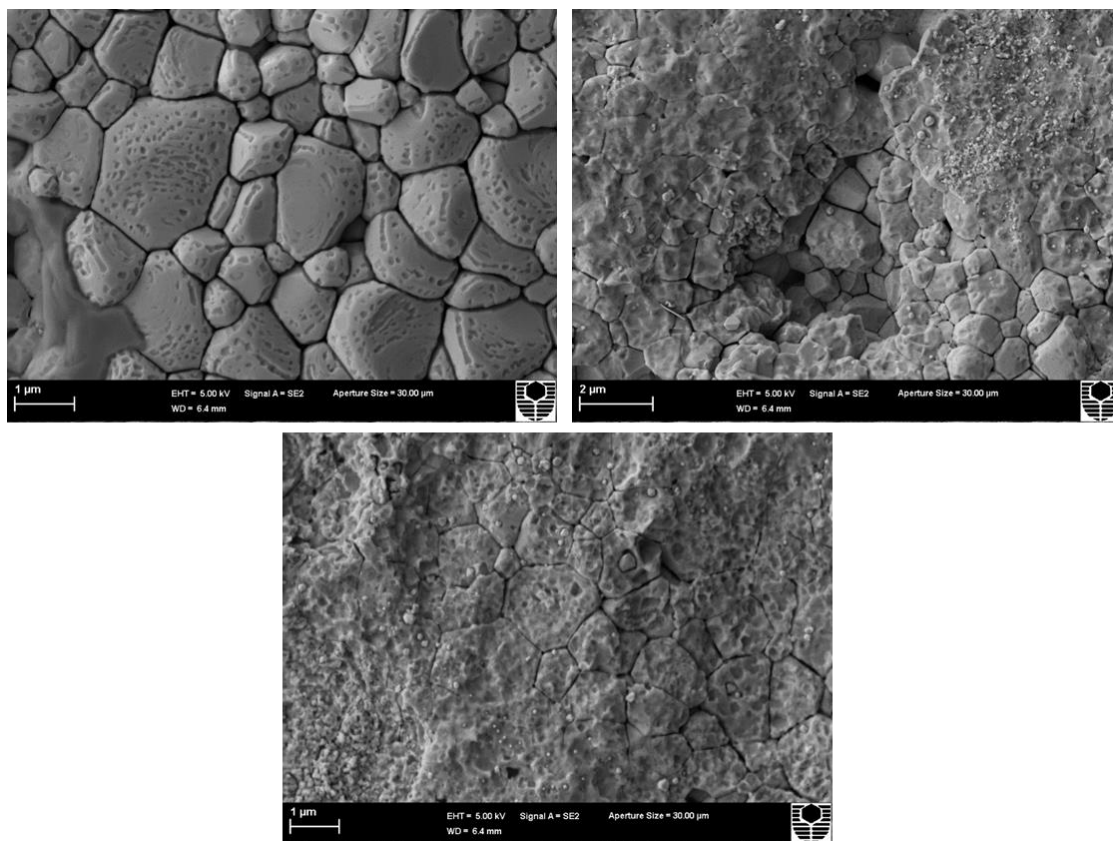


Figure 32 SEM images of LSCF-ESB applied on GDC after cathode removal through acid treatment. A: GDC particles; B and C: LSCF particles on GDC substrate.

In both samples different shapes can be distinguished: the underneath layer with clear grains and grain boundaries is the GDC electrolyte; then two different types of particles can be noted. The particles with a more regular and longer strip or needle-shaped particles are most likely the ESB; the other particles with an irregular shape are the LSCF electrode phase, see Figure 32. The LSCF particles cover the ESB and some of ESB may be migrated to the electrolyte surface under the influence of polarization.

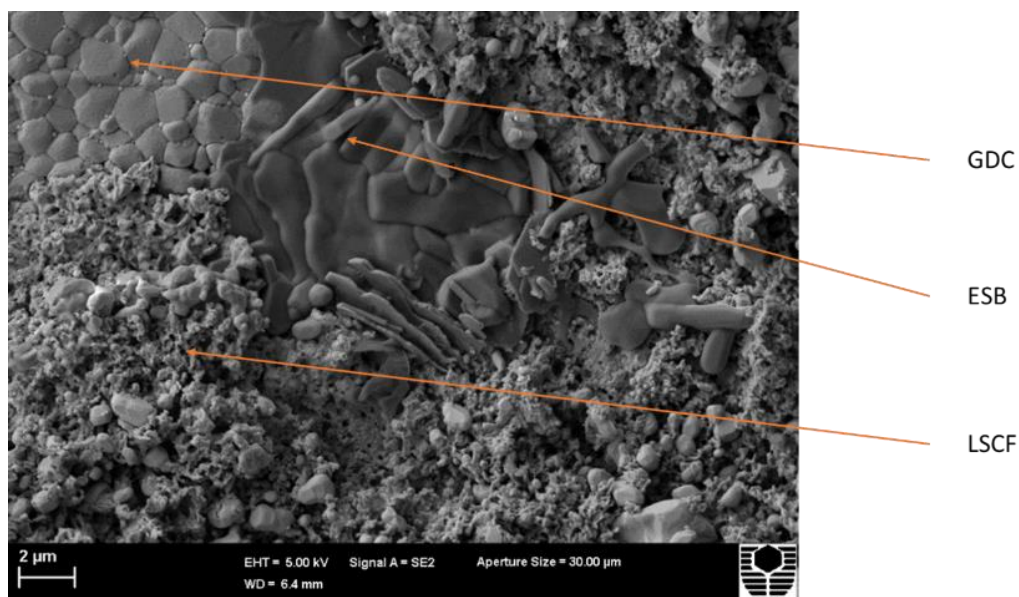


Figure 33 Particular of SEM images of LSCF-ESB applied on GDC after cathode removal through adhesive tape

The LSCF-ESB/GDC sample was further analysed by FIB-STEM and the results are shown in Figure 34 for the position A: this point was chosen due to the good interface between electrode and electrolyte; it was possible to note the sought segregation and migration of Erbium and Bismuth. There is a migration of ESB particles towards the interface between electrode and electrolyte, forming a rather dense bismuth layer at the interface. Erbium on the other hand is much less mobile as compared to the bismuth. However, different from the pristine LSCF/GDC interface (Figure 37), a clear segregation and migration of Sr at the GDC surface is also observed. The migration of Sr may be related to the bismuth as Sr is also a common dopant for bismuth oxides. The formation of dense bismuth layer is most likely due to an effect of polarization current and the result is the reduction of the resistance showed in the electrochemical impedance spectroscopy section of this work.

As mentioned before, figure 37 shows the TEM images and element distribution of uncontaminated LSCF (without adding ESB): the results do not show the strontium segregation obtained in the position A in figure 34.

Figure 35 shows the TEM images and element distribution of LSCF-ESB/GDC interface taking at position B: analysing this second point the same segregation and migration of erbium and bismuth of point A was noted, but there was not a clear migration of strontium.

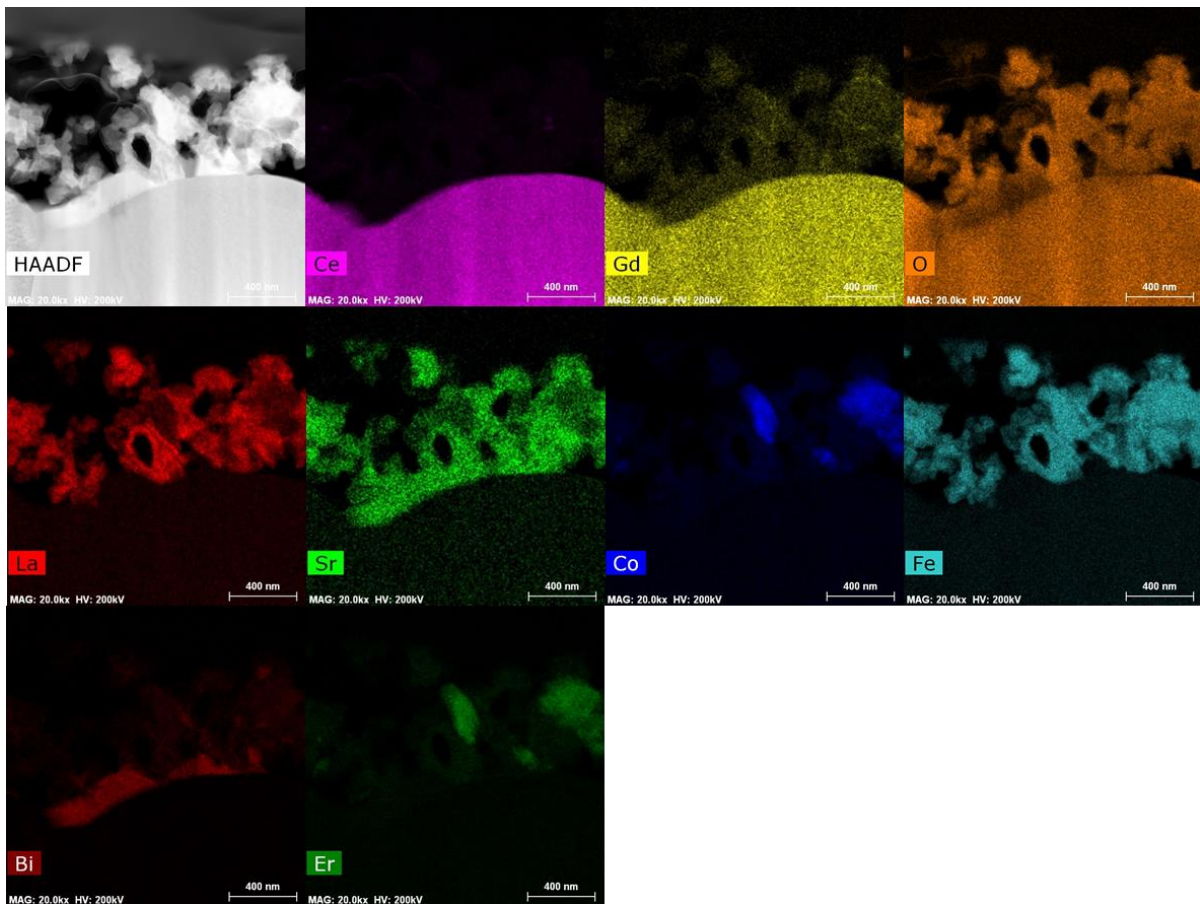


Figure 34 TEM images of LSCF-ESB applied on GDC point A

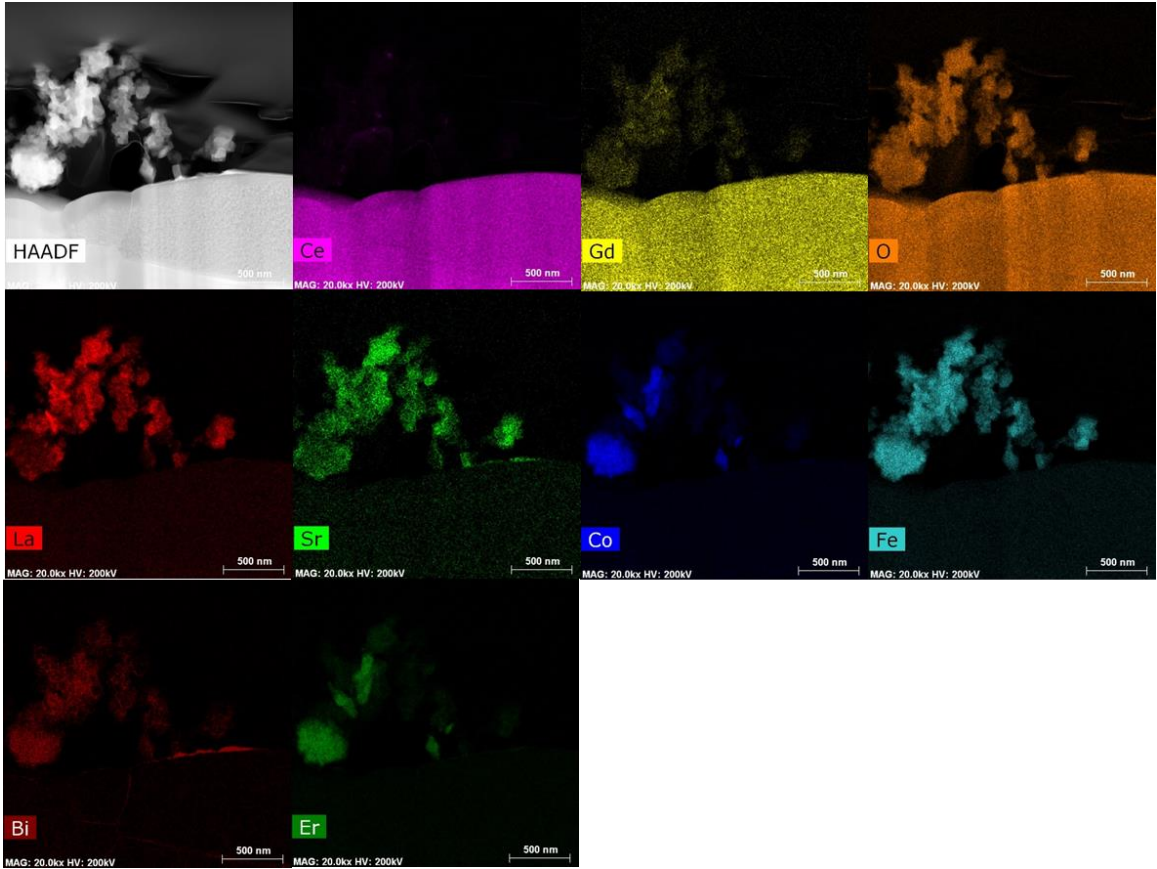


Figure 35 TEM images of LSCF-ESB applied on GDC point B

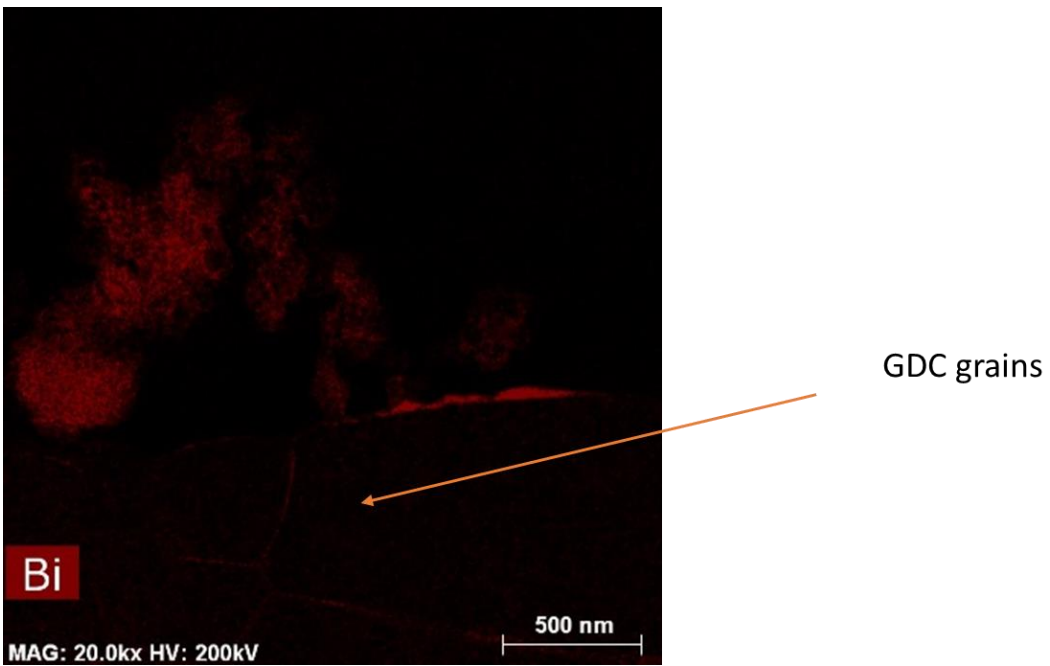


Figure 36 Particular of TEM images of LSCF-ESB applied on GDC point B

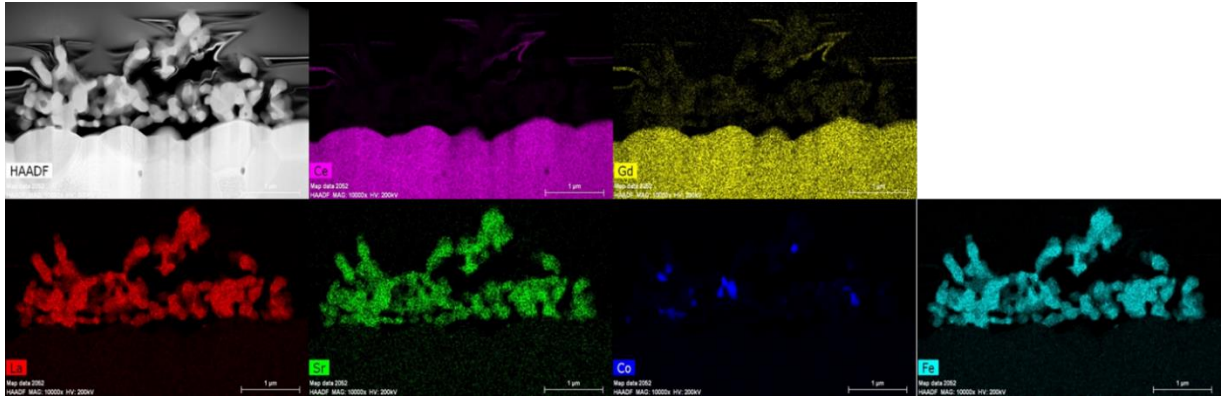


Figure 37: TEM images of LSCF applied on GDC

Figure 38 shows the TEM images of the LSCF-ESB/GDC interface after cathodic polarization treatment. As shown in Figure 38, GDC on the left and electrode particles on the right can be distinguished.

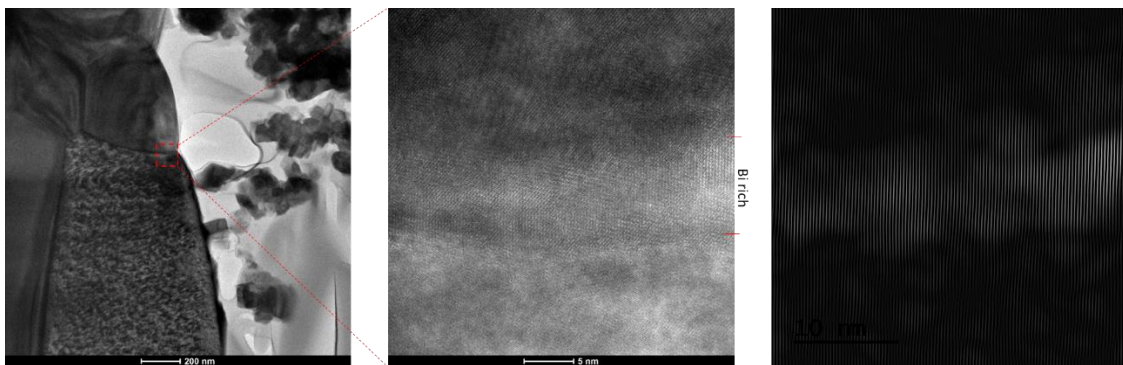


Figure 38 TEM images of LSCF-ESB applied on GDC

The central image is an enlargement of the red square: an area characterized by different index of phase can be distinguished in the central zone. This indicates the penetration of bismuth into the GDC grains after the cathodic polarization treatment. The third image is obtained with IFFT and better shows the different phase index in the area with the bismuth penetration. This behaviour can explain

the formation of a bismuth rich interface between GDC and the cathode: the ESB, bismuth in particular, as shown by figure 38 merges towards the interface forming a new layer. This layer will improve the connection between electrode and electrolyte, reducing the resistance and the losses.

6. Conclusion

Reversible Solid Oxide Cells are electrochemical devices able to convert chemical energy directly into electrical energy, reducing the losses of electricity generation through a thermodynamic cycle and the pollutant production. RSOCs operate now at high temperature, in the order of magnitude of 1000 °C: this temperature generates difficulties in the heat management due to large thermal flux produced during fuel cell mode operations. A possible solution is to reduce the operating temperature, trying to maintain the losses due to ohmic overvoltage to a low level. The results show that reducing the temperature from 750 °C to 600°C, there is an enlargement of R_{ohm} from $1,24 \Omega cm^2$ to $2,97 \Omega cm^2$ (LSCF-ESB on GDC sample, figure 25). The resistance can be kept constant, or anyway with a similar value, improving the interface connection between electrode and electrolyte: the aim of this study was to create and improve the interface through cathodic polarization treatment. Lanthanum Strontium Cobaltite Ferrite (LSCF) decorated with Erbium-Stabilized Bismuth (ESB) directly applied on Gadolinium-Doped Ceria (GDC) electrolyte cell was fabricated, tested and analysed after 100 h of polarization with cathodic current of $1000 mAcm^{-2}$ at 750°C. The EIS results showed higher electrochemical performances respect to pristine LSCF applied on GDC: the one doped with ESB possess lower activation energy and lower ohmic resistance. The

lower value of activation energy shows that this cell could have higher performance at lower temperature in comparison with simple LSCF. The LSCF-ESB/GDC half-cell was tested in the electrochemical test station to obtain the polarization curve: a reduction of the electrode potential increasing the time was showed by the results. After the polarization, a migration of the bismuth of decorated ESB towards the interface between electrode and electrolyte was observed, forming a dense bismuth layer on the GDC electrolyte surface. On the other hand, erbium is much less mobile as compared to bismuth. The formation of bismuth layer also induces the segregation and migration of Sr to the interface. The results appear to indicate that the phase migration depends strongly on the nature of the elements. This study clearly demonstrates the occurrence of the phase migration and separation of decorated LSCF-ESB cathode under the influence of cathodic polarization conditions, which has significant implications for the fundamental understanding of the segregation, migration and reaction at the interface of rSOCs.

7. Acknowledgements

I sincerely thank Professor San Ping Jiang and Professor Massimo Santarelli for the opportunity offered to me and Ms Yi Sun for all the knowledge and the time she spent helping me. The work was performed at Technology Park, Curtin University, Perth.

8. Appendix

Table A

	mole%	MW [g/mol]	mole	MW%
La	0,6	138,91	0,03	83,346
Sr	0,4	87,62	0,02	35,048
Co	0,2	58,933	0,01	11,7866
Fe	0,8	55,845	0,04	44,676
O	3	15,999	-	47,997
LSCF	2	-	0,05	222,8536

	mole%	MW [g/mol]	mole	weight [g]
La(NO ₃) ₃ *H ₂ O	0,6	433	0,03	12,99
Sr(NO ₃) ₂	0,4	211,64	0,02	4,2328
Co(NO ₃) ₂ *H ₂ O	0,2	291,046	0,01	2,91046
Fe(NO ₃) ₃ *H ₂ O	0,8	404,024	0,04	16,16096

	mole%	MW [g/mol]	mole	weight [g]
LSCF	1	222,8536	0,05	-
metalions	2	174,8566	0,1	-
EDTA	2	292,23	0,1	29,223
CA	4	192,12	0,2	38,424

	mole%	ml/mol	mole	weight [ml]
28%NH ₃ *	2	600	0,1	60

Table B

LSCF [g]	1,2		ratio	
ESB [g]	0,8		1,5	

	mole%	MW [g/mol]	MW%	mole
Er	0,4	167,26	66,904	0,001
Bi	1,6	208,98	334,368	0,001
O	3	15,999	47,997	-
ESB	1	-	449,269	0,002

	mole%	MW [g/mol]	mole	weight [g]
Er(NO ₃) ₃ *5H ₂ O	0,4	443,37	0,00071227	0,316
Bi(NO ₃) ₃ *5H ₂ O	1,6	485,07	0,00284907	1,382

	mole%	MW [g/mol]	mole	weight [g]
ESB	1	449,269	0,00178067	-
metalions	2	401,272	0,00356134	-
EDTA	2	292,23	0,00356134	1,041
CA	3	192,12	0,00534201	1,026

	mole%	ml/mol	mole	weight [ml]
28%NH ₃ *	2	600	0,00356134	2,137

9. References

- [1] Eric D. Wachsman and Kang Taek Lee, "Lowering the Temperature of Solid Oxide Fuel Cells," *Science*, vol. 334, pp. 935-939, 2011.
- [2] Shuangyin Wang and San Ping Jiang, "Prospects of fuel cell technologies," *Natl. Sci. Rev.*, vol. 4, no. 2, pp. 163-166, 2017.
- [3] Ana Maria Ferriz, Alfonso Bernad, Mitja Mori, Sabina Fiorot, "End-of-life of fuel cell and hydrogen products: A state of the art," *International journal of hydrogen energy*, no. 44, pp. 12872-12879, 2019.
- [4] "Download Center - Terna," [Online]. Available: <https://www.terna.it/it>.
- [5] Domenico Ferrero, Martina Gamba, Andrea Lanzini, Massimo Santarelli, "Power-to-Gas Hydrogen: techno-economic assessment of processes towards a multi-purpose energy carrier," *ScienceDirect*, no. 101, pp. 50-57, 2016.
- [6] "Fuel cells and hydrogen joint undertaking," [Online]. Available: <https://www.fch.europa.eu/page/horizon-2020-projects-pillar>.
- [7] D. ". F. -. S. -. S. o. T.-c. a. E.-c. P. S. -. P. d. Torino, "Remote," [Online]. Available: <https://www.remote-euproject.eu/>.

- [8] "Next Generation PEM Electrolysers under New Extremes," [Online]. Available: <https://www.neptune-pem.eu/en/about-neptune-2/project-objectives>.
- [9] "REFLEX project," [Online]. Available: <https://www.reflex-energy.eu/>.
- [10] "Wikipedia," [Online]. Available: https://en.wikipedia.org/wiki/Solid_oxide_fuel_cell.
- [11] Kendall, Subhash C Singhal and Kevin, High Temperature Solid Oxide Fuel Cells: Fundamentals, Design and Applications, The Boulevard, Langford Lane, Kidlington Oxford OX5 1GB, UK: Elsevier Advanced Technology, 1993.
- [12] T. Ishihara, "Development of New Fast Oxide Ion Conductor and Application for Intermediate Temperature Solid Oxide Fuel Cells," *Bull. Chem. Soc. Jpn.*, vol. 79, no. 8, pp. 1155-1166, 2006.
- [13] K. S. Paramvir Kaur, "Review of perovskite-structure related cathode materials for solid oxide fuel cell," *Ceramic international*, 2019.
- [14] Na Ai, Shuai He, Na Li, Qi zhang, William D.A. Rickard, Kongfa Chen, Teng Zhang, San Ping Jiang, "Suppressed Sr segregation and performance of directly assembled $\text{La}_{0.6}\text{Sr}_{0.4}\text{Co}_{0.2}\text{Fe}_{0.8}\text{O}_{3-x}$ oxygen electrode on $\text{Y}_2\text{O}_3\text{-ZrO}_2$ electrolyte of solid oxide electrolysis cells," *Journal of Power Sources*, vol. 384, pp. 125-135, 2018.
- [15] A. Mineshige, J. Izutsu, M. Nakamura, K. Nigaki, J. Abe, M. Kobune, S. Fujii, and T. Yazawa, "Introduction of A-site deficiency into $\text{La}_{0.6}\text{Sr}_{0.4}\text{Co}_{0.2}\text{Fe}_{0.8}\text{O}_{3-d}$ and its effect on structure and conductivity," *Solid State Ionics*, vol. 176, p. 1145-1149, 2005.

- [16] Shuai He, Qi Zhang, Giulio Maurizio, Lorenzo Catellani, Kongfa Chen, Qibing Chang, Massimo Santarelli and San Ping Jiang, "In Situ Formation of Er_{0.4}Bi_{1.6}O₃ Protective Layer at Cobaltite Cathode/Y₂O₃-ZrO₂ Electrolyte Interface under Solid Oxide Fuel Cell Operation Conditions," *ACS Appl. Mater. Interfaces*, vol. 10, pp. 40549-40559, 2018.
- [17] H. T. Hideaki Inaba, "Cerium-based solid electrolytes," *Solid State Ionics*, no. 83, pp. 1-16, 1996.
- [18] Jun Zhang, Christian Lenser, Norbert H. Menzler, Olivier Guillion, "Comparison of solid oxide fuel cell (SOFC) electrolyte materials for operation at 500 °C," *Solid State Ionics*, no. 344, p. 115138, 2020.
- [19] Srikar Mediseti, Junsung Ahn, Sunaina Patil, Apoorva Goel, Yaswanth Bangaru, Gautam V. Sabhahit, G. Uday Baskar Babu, Jong-Ho-Lee, Hari Prasad Dasari, "Synthesis of GDC electrolyte material for IT-SOFCs using glucose & fructose and its characterization," *Nano-Structures & Nano-Objects*, no. 11, pp. 7-12, 2017.
- [20] R. O. Fuentes, R. T. Baker, "Synthesis and properties of Gadolinium-doped ceria solid solution for IT-SOFC electrolytes," *International Journal of Hydrogen Energy*, vol. 33, no. 13, pp. 3480-3484, 2008.
- [21] J. E. Bauerle, "Study of Solid Electrolyte Polarization by a Complex Admittance Method," *J. Phys. Chem. Solids*, vol. 30, pp. 2657-2670, 1969.
- [22] Frank A. de Bruijn, Robert C. Makkus, Ronald K. A. M. Mallant, Gaby J. M. Janssen, "Materials for State-of-the-Art PEM Fuel Cells, and Their Suitability for Operation Above 100°C," *ScienceDirect*, vol. 1, pp. 235-336, 2007.

[23] "Shell opens third demo hydrogen station in LA region, at Toyota," *Fuel Cells Bulletin*, vol. 2011, no. 6, p. 7, 2011.

[24] PaoloColbertaldo Stacey, Britni Agustin, Stefano Campanari, Jack Brouwer, "Impact of hydrogen energy storage on California electric power system: Towards 100% renewable electricity," *International Journal of Hydrogen Energy*, vol. 44, no. 19, pp. 9558-9576, 2019.